



# Simulation of storm surge, wave, currents, and inundation in the Outer Banks and Chesapeake Bay during Hurricane Isabel in 2003: The importance of waves

Y. Peter Sheng,<sup>1</sup> Vadim Alymov,<sup>1</sup> and Vladimir A. Paramygin<sup>1</sup>

Received 24 March 2009; revised 7 October 2009; accepted 22 October 2009; published 7 April 2010.

[1] This paper investigates the effects of waves on storm surge, currents, and inundation in the Outer Banks and Chesapeake Bay during Hurricane Isabel in 2003 through detailed comparison between observed wind, wave, surge, and inundation data and results from an integrated storm surge modeling system, CH3D-SSMS. CH3D-SSMS, which includes coupled coastal and basin-scale storm surge and wave models, successfully simulated measured winds, waves, storm surge, currents, and inundation during Isabel.

Comprehensive modeling and data analysis revealed noticeable effects of waves on storm surge, currents, and inundation. Among the processes that represent wave effects, radiation stress (outside the estuaries) and wave-induced stress (outside and inside the estuaries) are more important than wave-induced bottom stress in affecting the water level.

Maximum surge was 3 m, while maximum wave height was 20 m offshore and 2.5 m inside the Chesapeake Bay, where the maximum wave-induced water level reached 1 m. Significant waves reached 3.5 m and 16 s at Duck Pier, North Carolina, and 1.6 m and 5 s at Gloucester, Virginia. At Duck, wave effects accounted for ~36 cm or 20% of the peak surge elevation of 1.71 m. Inside the Chesapeake Bay, wave effects account for 5–10% of observed peak surge level. A two-layer flow is found at Kitty Hawk, North Carolina, during the peak of storm surge owing to the combined effects of wind and wave breaking. Higher surge elevations result when the 3-D surge model, instead of the 2-D surge model, is coupled with the 2-D wave model owing to its relatively lower bottom friction.

Wave heights obtained with 3- and 2-D surge models show little difference.

**Citation:** Sheng, Y. P., V. Alymov, and V. A. Paramygin (2010), Simulation of storm surge, wave, currents, and inundation in the Outer Banks and Chesapeake Bay during Hurricane Isabel in 2003: The importance of waves, *J. Geophys. Res.*, *115*, C04008, doi:10.1029/2009JC005402.

## 1. Introduction

### 1.1. Storm Surge Modeling

[2] The major damage caused by hurricanes is associated with storm surges and coastal flooding. A storm surge is a huge mass of water, tens to hundreds km wide, that sweeps across the coastline where a hurricane makes landfall. The peak storm surge level can reach more than 3 m. The surge of high water topped by waves can be devastating. Along the coast, storm surge is the greatest threat to life and property. Accurate prediction of storm surge and coastal flooding is essential for developing cost effective storm mitigation and preparation.

[3] Numerous numerical models have been developed to simulate storm surges [e.g., Sheng, 1987, 1990; Flather, 1994; Jelesnianski *et al.*, 1992; Luettich *et al.*, 1992; Hubbert and McInnes, 1999; Casulli and Walters, 2000;

Sheng *et al.*, 2006]. Bode and Hardy [1997] reviewed the status of storm surge modeling.

[4] The accuracy of storm surge simulations depends on many factors: (1) input data (e.g., bathymetry, topography, and wind/pressure fields), (2) representation of important processes (e.g., flooding and drying, bottom friction, and effects of wave and tide), (3) model grid resolution, and (4) open boundary conditions. For example, Houston *et al.* [1999] compared the storm surge simulations produced by using the HRD wind field and the SLOSH wind field. Hubbert and McInnes [1999] showed that their model overestimated storm surge by 17% if the “flooding and drying” feature of their model is turned off owing to water piled up near the coast by the action of high wind and not allowing the water to propagate inland. Mastenbroek *et al.* [1993] and Zhang and Li [1996] showed that including wave-dependent surface wind stress significantly improved the surge height prediction. Shen *et al.* [2006] simulated diagnostically the effect of offshore surge on storm tide inside the Chesapeake Bay, without considering the effect of waves. Morey *et al.* [2006] showed that it is important to use a large model domain to incorporate the effect of remote forcing contribution to storm surge during Hurricane Dennis.

<sup>1</sup>Civil and Coastal Engineering Department, University of Florida, Gainesville, Florida, USA.

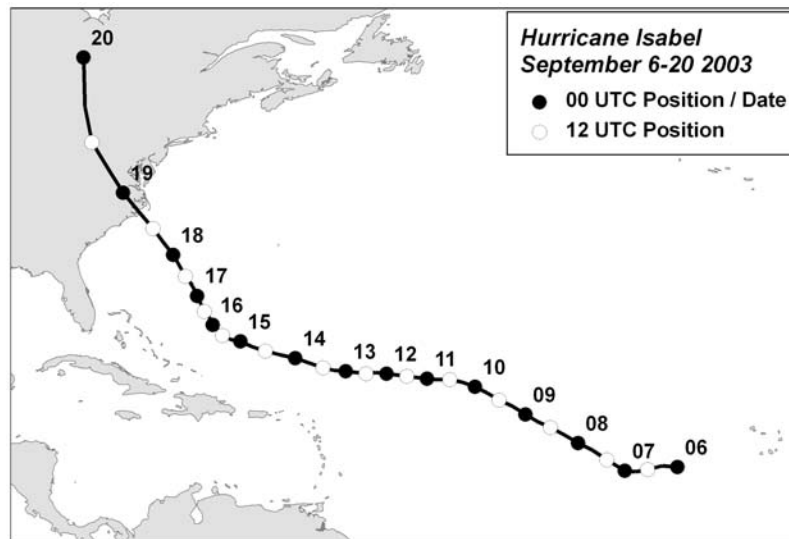


**Figure 1.** Best track of Hurricane Isabel. (Courtesy of the NOAA National Hurricane Center.)

*Interagency Performance Evaluation Taskforce (IPET)* [2006] simulated the storm surge and wave during Hurricane Katrina. *Zhang and Sheng* [2008] and *Lee and Sheng* [2008] simulated the storm surge and inundation during Ivan.

[5] This study aims to simulate the surge, wave, and inundation during Hurricane Isabel and to answer the following fundamental questions: How significantly does the wave affect storm surge? What is the relative importance of various wave processes (radiation stress, wave-induced drag, wave-induced bottom stress) in affecting storm surge and currents? Can a coupled 2-D wave model and a 3-D surge model simulate the vertical flow structure in coastal and estuarine water during hurricanes? Can a 2-D wave model accurately simulate the wave in coastal and estuarine water during hurricanes? To answer these questions, we use an integrated storm surge modeling system, CH3D-SSMS (see <http://ch3d-ssms.coastal.ufl.edu> and *Sheng et al.* [2006]), to conduct a comprehensive sensitivity study to simulate the storm surge and wave effects in the Outer Banks and Chesapeake Bay during Hurricane Isabel. Since wave effects cannot be easily extracted from the field data in such a complex environment, the integrated modeling system enables numerous model simulations to ensure that wind, wave, and water elevation can all be accurately simulated so that the wave effect can be accurately quantified.

## 1.2. Hurricane Isabel

[6] Hurricane Isabel of 2003, the track for which is shown in Figure 1, is considered one of the most significant tropical cyclones to affect portions of northeastern North Carolina and east-central Virginia since Hurricane Hazel of 1954 and the Chesapeake-Potomac Hurricane of 1933. The hurricane reached Category 5 status on the Saffir-Simpson Hurricane Scale. It made landfall near Drum Inlet on the Outer Banks of North Carolina as a Category 2 hurricane around 1730 UT on 18 September. According to *NOAA* [2004], 51 people died as a result of the storm (17 directly), with an official damage estimate of \$3.37 billion. Most of

the losses were incurred by Virginia (\$925M), Maryland (\$410M), and North Carolina (\$170M).

[7] Isabel brought hurricane conditions to portions of eastern North Carolina and southeastern Virginia. According to *NOAA's* National Hurricane Center, the highest observed sustained wind over land was 35 m/s with gusts up to 44 m/s at an instrumented tower near Cape Hatteras, North Carolina, at 1622 UT on 18 September. Another tower in Elizabeth City, North Carolina, reported 33 m/s sustained wind with a gust to 43 m/s at 1853 UT that day. The National Ocean Service station at Cape Hatteras reported 35 m/s sustained wind with a gust to 43 m/s before contact was lost. The Coastal Marine Automated Stations (C-MAN) at Chesapeake Light, Virginia, and Duck, North Carolina, reported similar winds. However, the wind record from the most seriously affected areas is incomplete, as several observing stations were destroyed or lost power as Isabel passed.

[8] According to *NOAA* [2004], the storm surge during Hurricane Isabel reached 2.5 m along the Outer Banks, 1.3 m at Duck, North Carolina, and almost 2.5 m in the upper Chesapeake Bay, generally 0.3 to 1.0 m higher than the *NOAA SLOSH* forecast that did not include any wave effect. During Isabel, waves were 12–15 m near the Outer Banks, a chain of emergent barrier islands separating the mainland from the Atlantic Ocean. Figure 2 shows the Isabel track and locations of all data stations for this study. It should be noted that, throughout this paper, water level will be reported in NAVD88 vertical datum unless otherwise noted. There have been a few studies investigating the effect of the hurricane on the Outer Banks and Chesapeake Bay. *Valle-Levinson et al.* [2002] studied the response of Chesapeake Bay circulation and salinity to Hurricane Floyd. *Preller et al.* [2005] applied the PCTides tide-surge forecast system, which is composed of a 2-D barotropic ocean model driven by tidal forcing and wind, to study the response of the ocean to Isabel in the Outer Banks and Chesapeake Bay areas. Using forecast wind fields produced by *NOGAPS*, *COAMPS* and analytical wind model, they simulated and

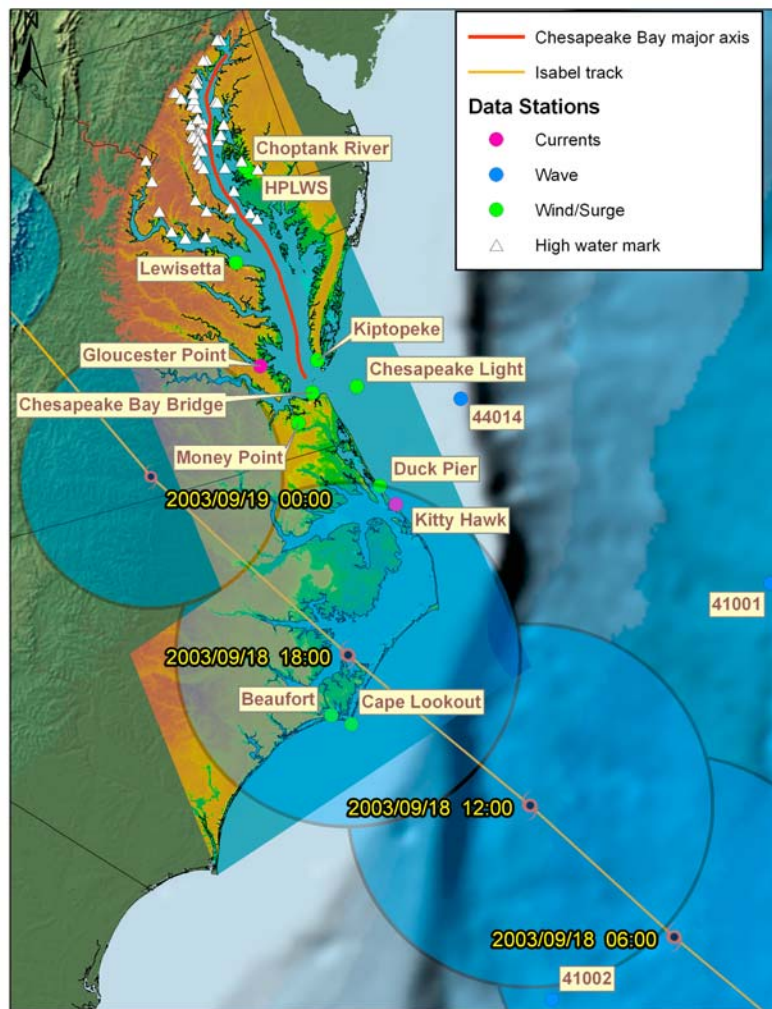


**Figure 2.** Isabel track showing locations of measured data and definition of the Chesapeake Bay major axis. Light blue circles represent radiuses of maximum wind at each time.

compared the water elevation to observed water elevation at eight locations throughout the computational domain with 3 km grid spacing. *Shen et al.* [2006] simulated storm tide in the Chesapeake Bay using an unstructured grid model UnTRIM. The model was forced by nine tidal harmonic constituents at the open boundary and an analytical wind field. A hindcast simulation of Isabel was able to capture peak storm tide and surge evolution at various sites of the Chesapeake Bay. Their study showed that the high surge in the upper Chesapeake Bay was caused by the forced southerly wind, while offshore surge and southeasterly and northeasterly winds contributed to surge in the lower Chesapeake Bay. *Li et al.* [2006] observed the phenomenon of complete destratification during Isabel in the main channel of the Chesapeake Bay. C. D. Rowley et al. ([http://www.nrl.navy.mil/Review06/images/06Simulation\(Rowley\).pdf](http://www.nrl.navy.mil/Review06/images/06Simulation(Rowley).pdf)) simulated the storm surge, tide, and dune erosion and breaching at Cape Hatteras National Seashore during Isabel. However, none of the previous studies considered the effect of wave on storm surge and inundation. This study simulates the storm surge, wave, and

inundation during Isabel and answers the fundamental questions raised in section 1.

[9] A very brief description of the integrated storm surge modeling system CH3D-SSMS is first given in the following. Observed water elevation in the Outer Banks and Chesapeake Bay during Hurricane Isabel are then compared with those simulated by CH3D-SSMS. Results of model simulations are then presented to quantify the effects of wave processes: radiation stress, wave-induced surface stress, and wave-induced bottom friction on storm surge.

## 2. An Integrated Storm Surge Modeling System: CH3D-SSMS

### 2.1. CH3D-SSMS

[10] CH3D-SSMS (see <http://ch3d-ssms.coastal.ufl.edu> and *Sheng et al.* [2006]), the storm surge modeling system used for this study, is composed of a local/coastal surge model, CH3D, and a local/coastal wave model, SWAN, which are coupled to a regional/basin-scale surge model, ADCIRC or UFDVM, and a regional/basin-scale wave mode, WW3.

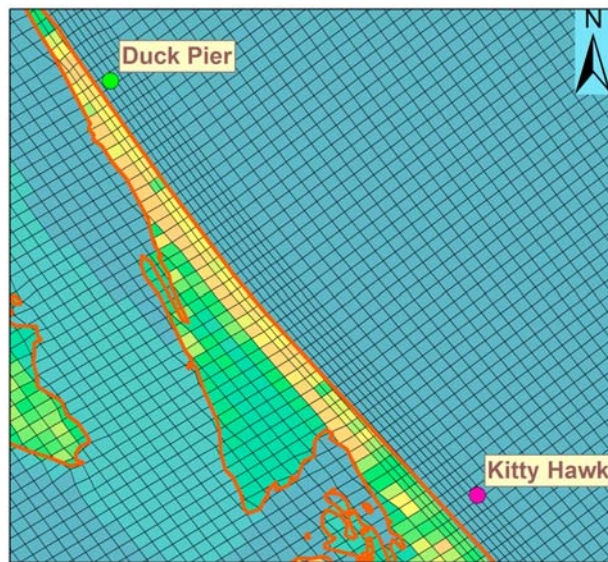


**Figure 3.** CH3D/SWAN grid zoom-in into Duck Pier and Kitty Hawk.

[11] The Curvilinear-Grid Hydrodynamics in 3-D (CH3D) model was originally developed by Sheng [1987, 1990]. The governing equations for CH3D are based on the wave- and Reynolds-averaged Navier-Stokes equations in a horizontally boundary-fitted curvilinear grid and a vertically terrain-following sigma grid, with assumptions of incompressible water, hydrostatic pressure, Boussinesq approximation and eddy-viscosity concept. The nonorthogonal boundary-fitted grid enables CH3D to more accurately represent the complex geometry than orthogonal grids used by such models as POM [Blumberg and Mellor, 1987] and ROMS [Song and Haidvogel, 1994]. CH3D uses a second-order closure turbulence model [Sheng and Villaret, 1989] for vertical turbulent mixing, and Smagorinsky-type horizontal eddy coefficients. Recent additions to the CH3D features include flooding and drying [e.g., Davis and Sheng, 2003], wave-induced radiation stress, wave-current bottom stress [Sheng and Villaret, 1989; Alymov, 2005], and wave-induced surface stress [Alymov, 2005].

[12] CH3D-SSMS has been used to simulate many of the hurricanes during 2003–2005 as well to provide real-time forecast of hurricane wind, storm surge, wave, and coastal inundation for various regions along the Gulf and Atlantic coasts. In this study, only hindcasting simulation of Isabel will be presented with a main focus on the sensitivity of model results to wind fields and model process formulation, particularly wave effects and 3-D effects. The governing equations of CH3D in Cartesian and boundary-fitted non-orthogonal curvilinear coordinates, along with boundary conditions, are given in Appendix A.

[13] Because of the use of an efficient conjugate gradient solver for solving the external mode of CH3D semi-implicitly, a relatively large time step (60–120 s) can generally be used with a minimum horizontal grid spacing of 25–50 m in the coastal domain. However, CH3D is not used for the basin-scale surge simulation in the Atlantic and Gulf coasts, because that would require too many grid cells

and hence a huge increase in computational resources. Rather, to achieve efficient simulation with limited computer resources, we couple CH3D in the coastal domain with a regional/basin-scale surge model (e.g., ADCIRC) that uses a relatively coarse grid. A typical hurricane simulation by CH3D-SSMS requires approximately 1–2 h (2-D) or 7–8 h (3-D) on a single-CPU Dell computer (3.2 GHz), using a high-resolution grid (minimum spacing of 25 m, average spacing of 450 m, and maximum spacing of 1700 m) and less than 250,000 cells in the coastal domain of CH3D and a time step of approximately 60–120 s. The coastal domain as shown in Figure 2 has 548,240 grid cells. The track of Isabel and locations of data stations are also shown in Figure 2. As an example, Figure 3 shows the detailed CH3D grid in the vicinity of Duck, North Carolina.

[14] We use the 2-D vertically averaged version of ADCIRC [Luettich *et al.*, 1992; IPET, 2006] or UFDVM [Lee and Sheng, 2008] to simulate the regional/basin-scale surge over the entire Gulf of Mexico and western North Atlantic represented by the EC95d (ADCIRC Tidal Database, version ec\_95d; see <http://www.unc.edu/ims/ccats/tides/tides.htm>) grid with 31,435 nodes, and to provide water elevation along the open boundaries of the coastal surge model CH3D. The EC95d grid has a minimum spacing of 200 m, an average spacing of 3 km, and a maximum spacing of 25 km. With a time step of 30 s, it requires about 3 h for ADCIRC to simulate Isabel on a single CPU Dell with 3.2 GHz. If a high-resolution grid comparable to the CH3D grid in Figure 2 were used by ADCIRC, it would require a time step of 1 s and prohibitively long computational time on the single CPU Dell. To save computational time, we use CH3D with the high-resolution grid and ADCIRC with the coarse offshore grid. Tides along the CH3D open boundaries are provided by the ADCIRC tidal constituents [Mukai *et al.*, 2002].

[15] For wave simulation in the CH3D domain, we use the Simulating Waves Nearshore (SWAN) model [Booij *et al.*, 1999], a third-generation wave model which computes random, short-crested wind-generated waves in coastal regions and inland waters. SWAN accounts for wave propagation in time and space, shoaling, refraction owing to current and depth, frequency shifting owing to currents and nonstationary depth, wave generation by wind, bottom friction, depth-induced breaking, and transmission through and reflection from obstacles. SWAN can use the exact model domain and curvilinear grid of CH3D, thus allowing the two models to achieve dynamic coupling without having to spatially interpolate the results of one model to another. Since SWAN is not considered a robust model for the deep water, we use the model results of WAVEWATCH-III (WW3) to provide the wave conditions along the open boundaries of the coastal CH3D/SWAN domain. SWAN executes much slower than CH3D, hence in this study it is run every 20 min to save computational time. While nonstationary SWAN (with small time step of up to 3 s) should generally be used to simulate waves in a fast moving storm, the stationary SWAN was found to yield quite reasonable wave conditions versus data in a rather slow moving storm such as Isabel. In fact, the nonstationary SWAN yielded results that are comparable to the stationary SWAN results.

**Table 1.** Parameters Used to Create the Lookup Table for Wave-Enhanced Bottom Stress

Parameter	Value
Water depth	0.5–5.0 m with 0.5 m increments
Wave height	0.0–2.0 m with 0.2 m increments
Wave period	2–16 s with 1 s increments
Wave direction	0–315 deg with 45 deg increments
Current	0.0–1.0 m/s with 0.1 m/s increments

[16] WAVEWATCH III, also known as WW3 [Tolman 1999], is a third-generation wave model developed at NOAA/NCEP in the spirit of the WAM model [The Wamdi Group, 1988; Komen *et al.*, 1994]. Two basic model assumptions limit the model application to spatial scales (grid increments) larger than 1 to 10 km and outside the surf zone. We use WW3 results to provide the wave conditions along the open boundaries of the CH3D/SWAN domain. The domain of the WW3 model is similar to the ADCIRC domain. WW3 uses the WNA wind, which is based on the GFDL hurricane wind model.

## 2.2. Modeling Current-Wave Interaction in Coastal Region

[17] In this study, three aspects of current-wave interaction are considered: (1) wave-induced radiation stress based on the formulation of Longuet-Higgins and Stewart [1964]; (2) wave-enhanced wind stress [Donelan *et al.*, 1993]; (3) wave-enhanced bottom stress (the modified Grant and Madsen [1979] formula developed by Signell *et al.* [1990]) and a bottom stress lookup table developed by Alymov [2005] using the turbulent boundary model of Sheng and Villaret [1989]; and (4) wave-enhanced turbulent mixing. A brief description of these four aspects, which are included in our model simulations, are given here.

### 2.2.1. Wave-Enhanced Surface Drag Coefficient and Roughness

[18] Wave-enhanced surface roughness,  $z_0$ , and drag coefficient,  $C_{de}$ , developed by Donelan *et al.* [1993], are used to calculate wind stress at the free surface (equations (1) and (2)). Both the surface roughness and the drag coefficient are functions of wave age. When waves are young the roughness increases making the wind stress higher as opposed to when waves are fully developed.

$$z_0 = 3.7 \cdot 10^{-5} \left( \frac{W_s^2}{g} \right) \left( \frac{W_s}{C_p} \right)^{0.9} \quad (1)$$

where  $W_s$  is the wind speed at 10 m above air–sea interface. Following the relation between  $z_0$  and  $C_{de}$ ,  $z_0 = z \cdot \exp(-\kappa/\sqrt{C_{de}(z)})$ , yields the wave-enhanced drag coefficient

$$C_{de} = \left[ \frac{\kappa}{z \ln \left( \frac{3.7 \cdot 10^{-5} \left( \frac{W_s^2}{g} \right) \left( \frac{W_s}{C_p} \right)^{0.9}}{z} \right)} \right]^2 \quad (2)$$

where  $C_p$  is wave phase speed and  $W_s/C_p$  represents the inverse wave age. Wave-induced wind stress is obtained by subtracting the wind stress in a wind-only (no wave) model simulation, where Garratt formula for  $C_d$  as shown in Appendix A is used, from the wave-enhanced wind stress in a simulation with both wind and wave.

### 2.2.2. Wave-Enhanced Bottom Stress

[19] Wave-enhanced bottom stress is implemented in CH3D using two methods. The first method uses a simplified formulation developed by Signell *et al.* [1990] on the basis of the Grant and Madsen [1979] theory for a wave-averaged bottom boundary layer, while the second method uses a comprehensive lookup table for wave–current bottom stress developed with a turbulent closure model of Sheng and Villaret [1989] for a wave-resolving turbulent wave–current boundary layer.

[20] The Grant and Madsen [1979] formulation is given by the typical quadratic law with one distinction where  $C_{de}$  is the wave-enhanced drag coefficient.

$$\tau_{bx} = \rho C_{de} u_b \sqrt{u_b^2 + v_b^2} \quad (3)$$

$$\tau_{by} = \rho C_{de} v_b \sqrt{u_b^2 + v_b^2} \quad (4)$$

[21] The main assumption used in the formulation is that for a colinear flow, the maximum bottom shear stress is defined as

$$\tau_{b,max} = \tau_c + \tau_w \quad (5)$$

where  $\tau_c$  is the bottom stress owing to current and  $\tau_w$  is the maximum stress owing to waves which can be determined from

$$\tau_w = \frac{1}{2} \rho f_w u_w^2 \quad (6)$$

where  $u_w$  is the near-bottom wave orbital velocity and  $f_w$  is the wave friction factor which depends on the bottom roughness,  $k_s$ . The final expression for the wave-enhanced drag coefficient at the reference height,  $z_r$ , chosen to lie above the wave boundary layer is

$$C_{de} = \left( \frac{\kappa}{\ln(30z_r/k_{bc})} \right)^2 \quad (7)$$

where  $k_{bc}$  is an apparent bottom roughness which includes the effect of wave [Grant and Madsen, 1979].

[22] Following Signell *et al.* [1990], where  $\kappa = 0.4$  is the von Karman constant, the reference height  $z_r$  was specified as 20 cm and  $k_s = 0.1$  cm was selected to correspond to a drag coefficient of  $1.5 \cdot 10^{-3}$  at one meter above the bed in the absence of waves. Once the effective drag coefficient  $C_{de}$  is calculated, it is used in CH3D to compute bottom stress as defined by equations (3) and (4).

[23] The second formulation uses a turbulent closure model [Sheng and Villaret, 1989] to calculate the wave–current bottom shear stress inside a turbulent wave–current bottom boundary layer. The wave-resolving governing

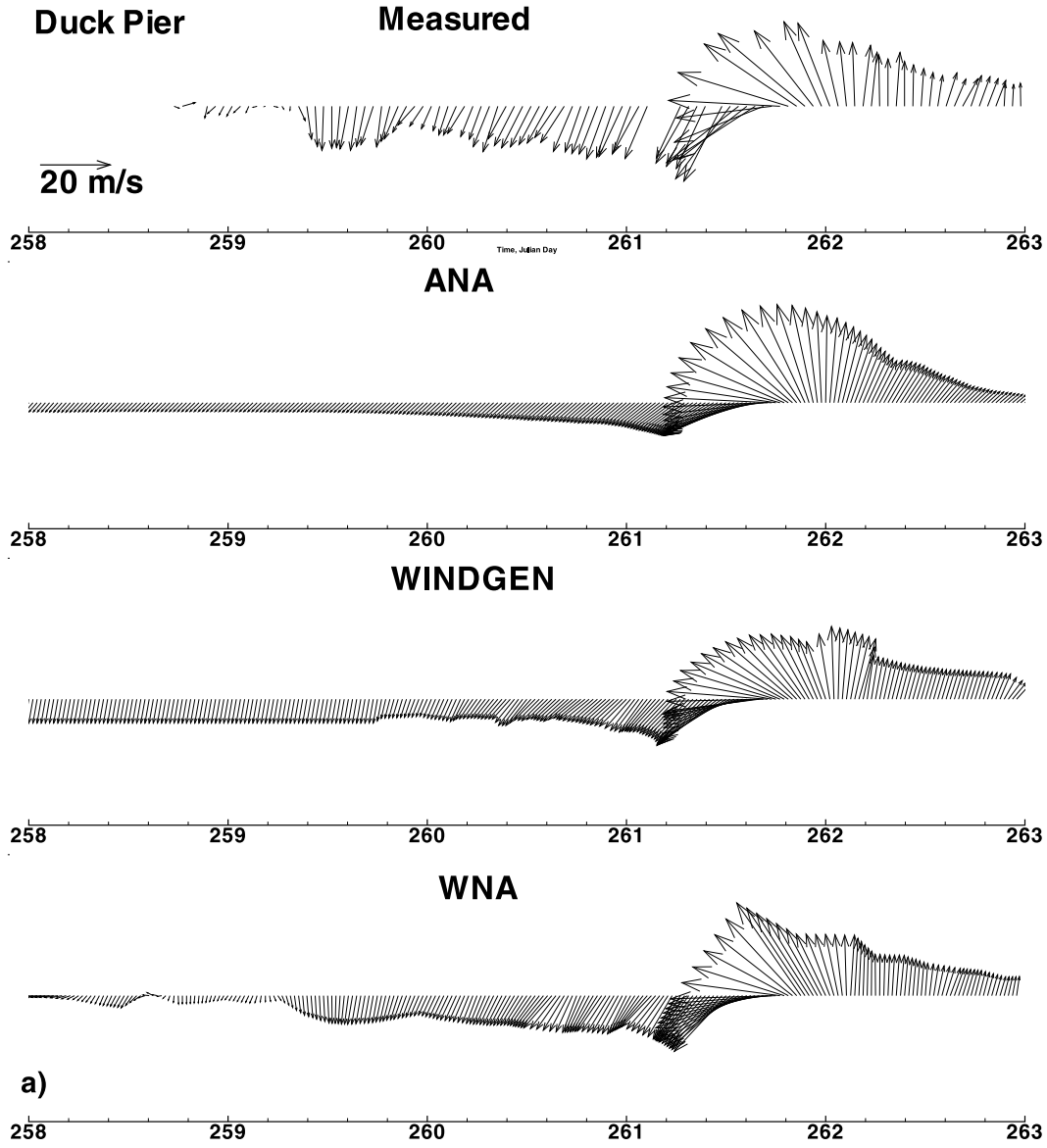


**Figure 4.** Measured/simulated wind at (a) Duck Pier, (b) Gloucester Point, (c) Cape Lookout, and (d) HPLWS.

equations for the combined wave–current bottom boundary layer are:

$$\frac{\partial u}{\partial t} = -\frac{1}{\rho} \frac{\partial p}{\partial x} + \frac{\partial}{\partial z} \left( A_v \frac{\partial u}{\partial z} \right) \quad (8)$$

$$\frac{\partial v}{\partial t} = -\frac{1}{\rho} \frac{\partial p}{\partial y} + \frac{\partial}{\partial z} \left( A_v \frac{\partial v}{\partial z} \right) \quad (9)$$

with the following bottom boundary conditions:

$$\tau_{bx} = A_v \frac{\partial u}{\partial z} = \rho C_d u_1 \sqrt{u_1^2 + v_1^2} \quad (10)$$

$$\tau_{by} = A_v \frac{\partial v}{\partial z} = \rho C_d v_1 \sqrt{u_1^2 + v_1^2} \quad (11)$$

where  $u_1$ ,  $v_1$  are velocity components at the lowest grid point,  $z_1$ , and  $C_d$  is computed by:

$$C_d = \left[ \frac{\kappa}{\ln(z_1/z_0)} \right]^2 \quad (12)$$

where  $z_0$  is the bottom roughness which was set to 0.1 cm. The smallest grid spacing near the bottom is 0.03 cm.

[24] Boundary conditions at the top of the bottom boundary layer, which was set to 30 cm, are:

$$\tau_{sx} = A_v \frac{\partial u}{\partial z} = 0 \quad (13)$$

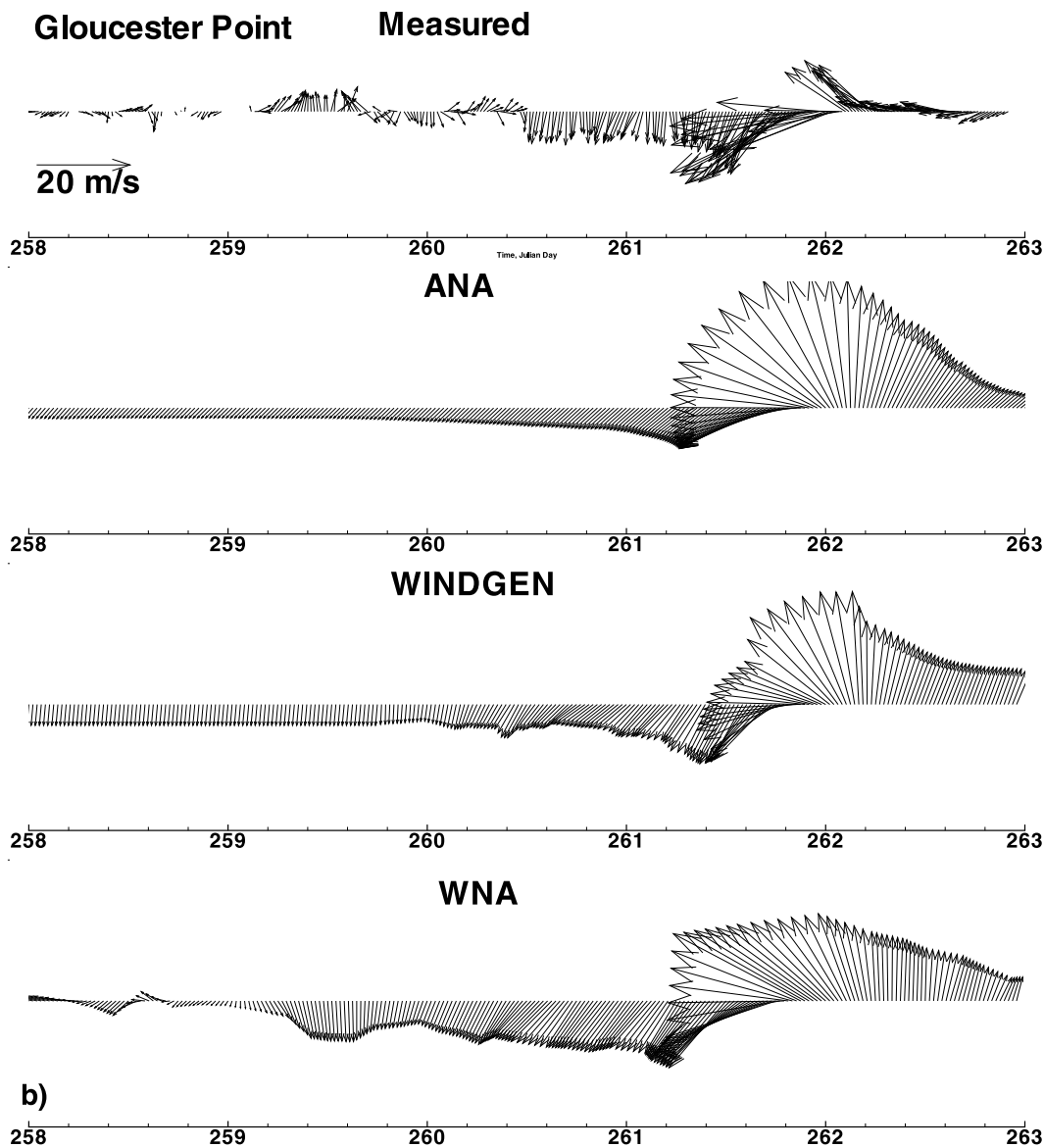


Figure 4. (continued)

$$\tau_{sy} = A_v \frac{\partial v}{\partial z} = 0 \quad (14)$$

[25] To drive a wave-induced oscillatory motion inside the boundary layer, a pressure gradient from the linear wave theory is applied:

$$\left( -\frac{1}{\rho} \frac{\partial p}{\partial x} \right)_w = \frac{1}{2} gkH \frac{\cosh(kz)}{\cosh(kh)} \sin \varphi \cos(\sigma t) \quad (15)$$

$$\left( -\frac{1}{\rho} \frac{\partial p}{\partial y} \right)_w = \frac{1}{2} gkH \frac{\cosh(kz)}{\cosh(kh)} \cos \varphi \cos(\sigma t) \quad (16)$$

where  $g$  is gravitational acceleration,  $k$  is wave number,  $H$  is wave height,  $\varphi$  is wave direction, and  $\sigma$  is angular wave frequency.

[26] To drive a current inside the boundary layer, a constant pressure gradient is applied in the  $y$  direction:

$$\left( -\frac{1}{\rho} \frac{\partial p}{\partial y} \right)_c = \text{const} \quad (17)$$

[27] The vertical turbulent eddy viscosity  $A_v$  inside the turbulent wave-current boundary layer is determined using a TKE closure model developed by *Sheng and Villaret* [1989] and a very small time step which is 1/100 of the wave period. A total of 145,200 model runs (see Table 1) are made, taking into account of various combinations of five different model parameters: water depth, wave height, wave period, wave direction and current magnitude. These runs resulted in a comprehensive lookup table of bottom shear stress in a wave-current boundary layer. During a CH3D simulation, the bottom stress value at each grid cell is determined by interpolation of the bottom stress values in

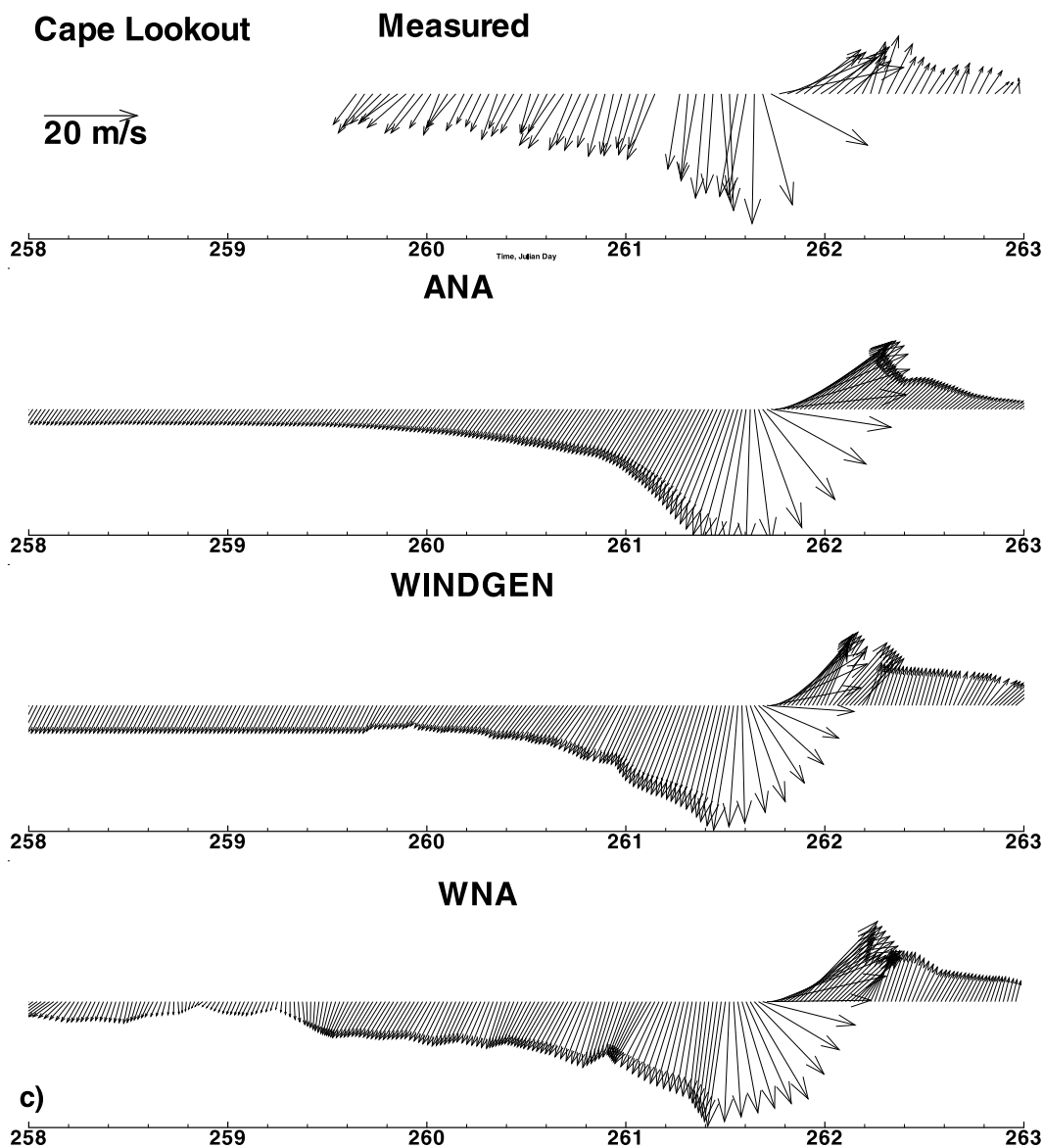


Figure 4. (continued)

the lookup table in a five-dimensional space (i.e., water depth, wave height, wave period, wave direction, current magnitude). The current is specified at the lowest grid point,  $z_1$ , where CH3D calculates its currents.

[28] Therefore, the water depth within the 1-D model is defined as half of the vertical grid spacing subtracted by the roughness length, and the wave height corresponded to the  $z_1$  point is determined according to the linear wave theory:

$$H_{(z=z_1)} = H_{(z=\zeta)} \frac{\sinh k(h+z_1)}{\sinh k(h+\zeta)} \quad (18)$$

where  $h$  is local water depth,  $\zeta$  is water surface elevation, and  $H_{(z=\zeta)}$  is wave height at the surface.

### 2.2.3. Wave-Induced Radiation Stress

[29] The CH3D governing equations as shown in Appendix A include wave-induced radiation stress terms which contribute to wave setup in the nearshore region.

Within CH3D, the classical formulation of *Longuet-Higgins and Stewart* [1964], which assumes vertically uniform radiation stress throughout the entire water column, plus a contribution owing to surface roller [Svendsen, 1987; Haas and Svendsen, 2000], which only exists in the top layer between the free surface and the wave trough, are implemented.

[30] The vertically uniform radiation stress terms are:

$$S_{xx} = E \left[ n(\cos^2 \theta + 1) - \frac{1}{2} \right] \quad (19)$$

$$S_{yy} = E \left[ n(\sin^2 \theta + 1) - \frac{1}{2} \right] \quad (20)$$

where  $E$  is total wave energy,  $\theta$  is angle between the direction of wave propagation and the  $x$  axis (representing

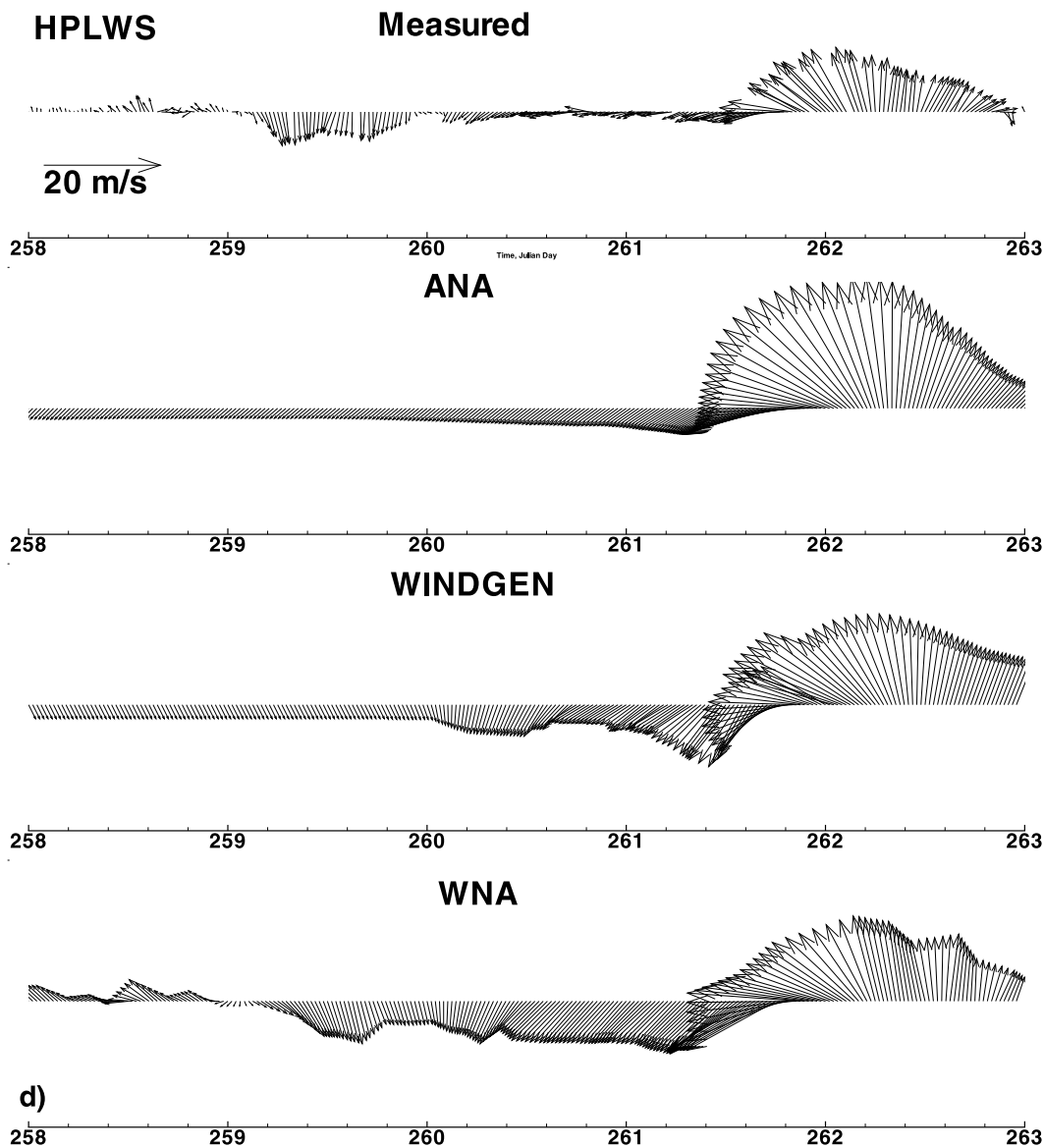


Figure 4. (continued)

onshore direction), and  $n$  is the ratio of group velocity to wave celerity.

[31] The radiation stress term representing the flux of the longshore component in the onshore direction is:

$$S_{xy} = \frac{E}{2} n \sin 2\theta \quad (21)$$

[32] While vertically varying radiation stress formulations have been developed, some formulation [Mellor, 2003] contains error and other [Mellor, 2008] requires additional effort for incorporation into the curvilinear-grid CH3D modeling system. Hence these formulations are not used in this study.

#### 2.2.4. Wave-Enhanced Turbulent Mixing

[33] For the vertical eddy viscosity, the equilibrium turbulence closure scheme developed by Sheng and Villaret

[1989] was modified to take into account wave effects. To take into account the wave effects, an additional term was added to the vertical eddy viscosity:

$$A_z = A_{zc} + Mh(D_b/\rho)^{1/3} \quad (22)$$

where  $A_{zc}$  is the eddy viscosity owing to the mean currents as computed by Sheng and Villaret's equilibrium closure model,  $D_b$  is the wave energy dissipation resulted from wave breaking and bottom friction,  $h$  is the water depth and  $M$  is a constant. The second term on the right-hand side of equation (22) represents the contribution to turbulence by waves, following Battjes [1975] and De Vriend and Stive [1987].

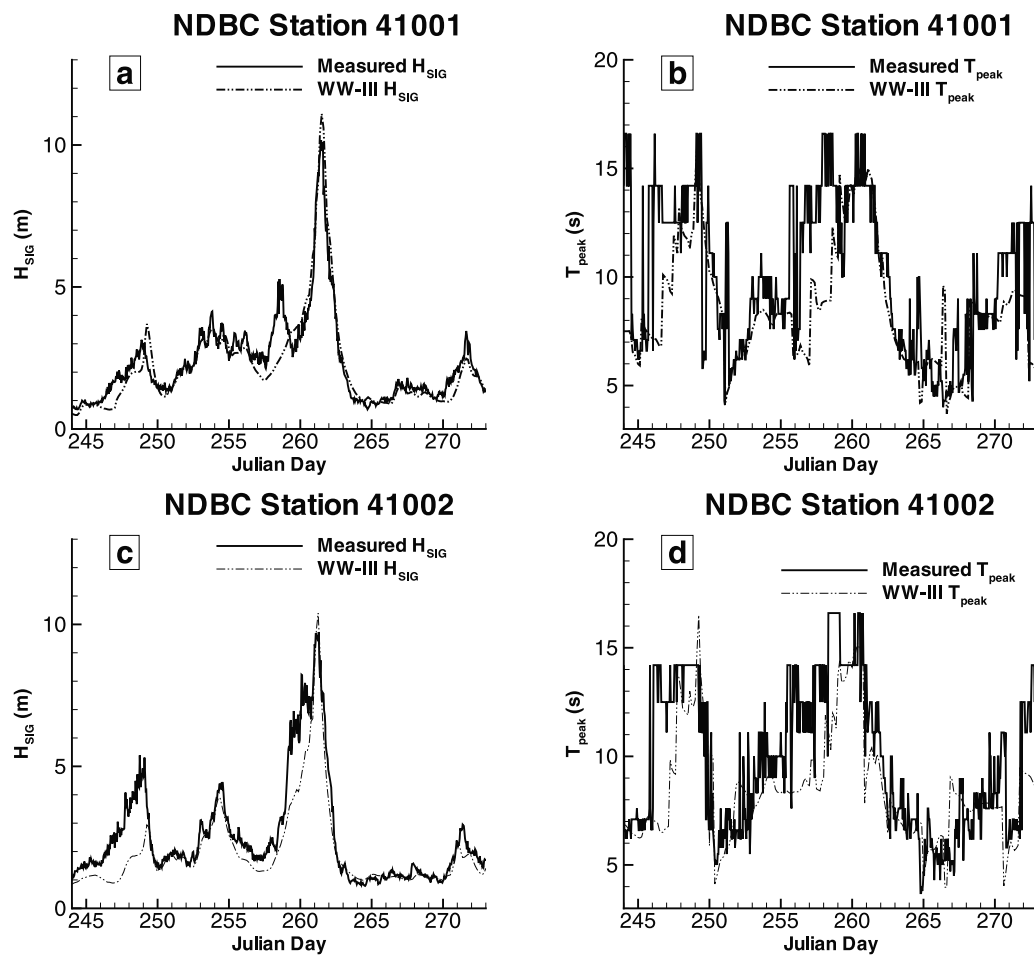


**Figure 5.** Measured and WW3 wave conditions at 41001 and 41002 along the open boundaries of SWAN/CH3D.

### 2.3. Coupling Coastal and Basin-Scale Surge and Wave Models

[34] In a CH3D-SSMS simulation, there is coupling between surge and wave models as well as coupling between local and regional models. Both one-way and two-way couplings are involved. In one-way coupling, such as between ADCIRC (model A) and CH3D (model B), results of model A are fed to model B whose results are not fed back to model A. Since the ADCIRC domain covers the western North Atlantic, the Gulf of Mexico and the Caribbean Sea, ADCIRC can provide water elevation along open boundaries of the CH3D domain during hurricane events even when the hurricane is located thousands of kilometers away. Both models are run concurrently using the same time step. ADCIRC results are not affected by results of CH3D. The same one-way coupling is used to couple WW3 and SWAN, where SWAN open boundary conditions (significant wave height, peak wave period and direction, etc) are provided by the WW3. CH3D and SWAN always use the same wind field; that is, either WNA, WGN (WINDGEN; see *Graber et al.* [2006]), or ANA (Analytical) [Holland, 1980].

[35] In two-way coupling between CH3D (model A) and SWAN (model B), results calculated by model A are

frequently fed to model B whose results are fed back to model A during a simulation. The exact steps are: (1) incorporating the updated water depths from the surge model into the wave model; (2) incorporating the updated currents from the surge model into the wave model; (3) including the wave effects on currents by the radiation stress terms in the surge model; and (4) including wave-current bottom stresses in the surge model. For CH3D simulation, wave-enhanced surface roughness and drag coefficient described in equations (1) and (2) are used. For simplicity, surge and wave coupling in the basin-scale models is not implemented.

[36] To enable seamless wave-surge coupling, CH3D and SWAN use the same boundary-fitted curvilinear grid which allows flooding and drying. However, since SWAN is quite time consuming, SWAN simulation is typically conducted every 20 min to ease the computational burden. This means that after twenty 60 s CH3D time steps, the two models mutually exchange information: CH3D receives wave information (wave height, wave period, and wave direction) to allow calculation of radiation stresses and wave setup, while SWAN, in return, updates bathymetry that has changed owing to tide, storm surge, wave setup, and inundation of previously dry areas. The current field used in the SWAN simulation gets updated, and the updated wind field is passed via CH3D. Isabel was a slow moving storm

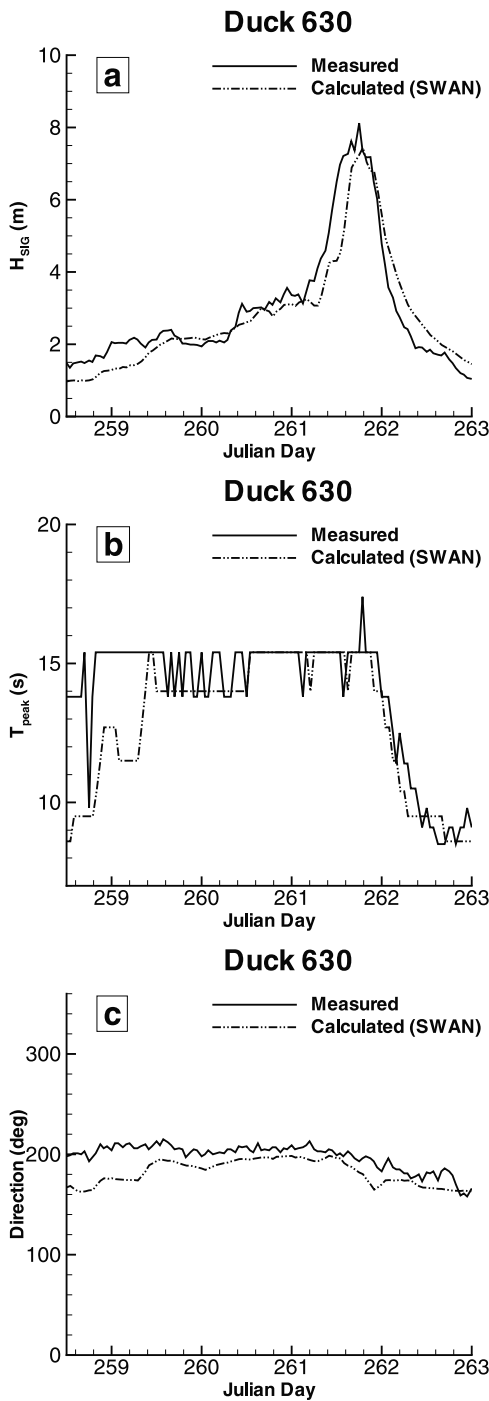


**Figure 6.** Measured versus SWAN simulated wave conditions at Duck 630.

(with a forward speed of around 6–8 kt as it was approaching the United States coast but increased to 15–20 kt after the storm landfall), so the change in wind speed and direction was not too abrupt in the open water. Hence the wave results simulated by stationary (run every 20 min) and nonstationary (with 3 min time step) SWAN were only slightly different, on the basis of comparison of the simulated significant wave height and period as well as energy spectra at several stations versus data at Duck. Perhaps other

reasons why nonstationary SWAN did not give very different results from the stationary SWAN simulation are related to (1) a significant amount of wind energy is allowed to cap during each SWAN step and (2) the boundary conditions for SWAN are provided by the WW3 model results which are available at 3 h intervals which are then linearly interpolated in time.

**2.4. Computational Domain: Outer Banks and Chesapeake Bay**

[37] Hurricane Isabel made landfall along the south Outer Banks area near Drum Inlet, North Carolina. The impact of Isabel, however, was spread out over a vast domain including east Outer Banks, Croatan-Albemarle-Pamlico Estuary System, and Chesapeake Bay. A computational grid that covers all the affected areas was created for CH3D and SWAN. As shown in Figure 2, the grid contains two open boundaries: the southern open boundary starts at Wilmington, North Carolina, and extends 300 km to the east where the continental shelf ends, while the eastern open boundary extends from there by 578 km to the north. Both open boundaries are far away from the coastline of the areas affected by Isabel. The distance from the south Outer Banks to the southern open boundary ranges from 40 to 80 km whereas the distance from the east Outer Banks to the eastern open boundary is between 40 and 60 km.

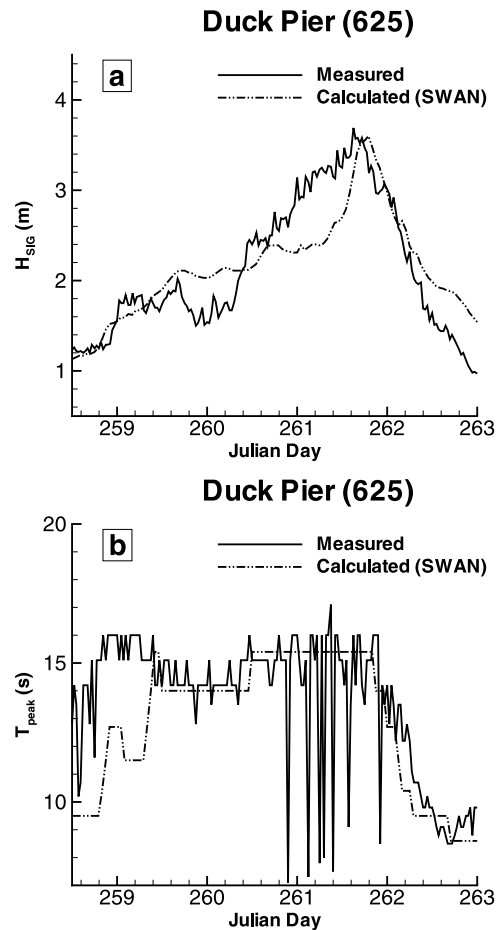


**Figure 7.** Measured versus SWAN simulated wave conditions at Duck 625.

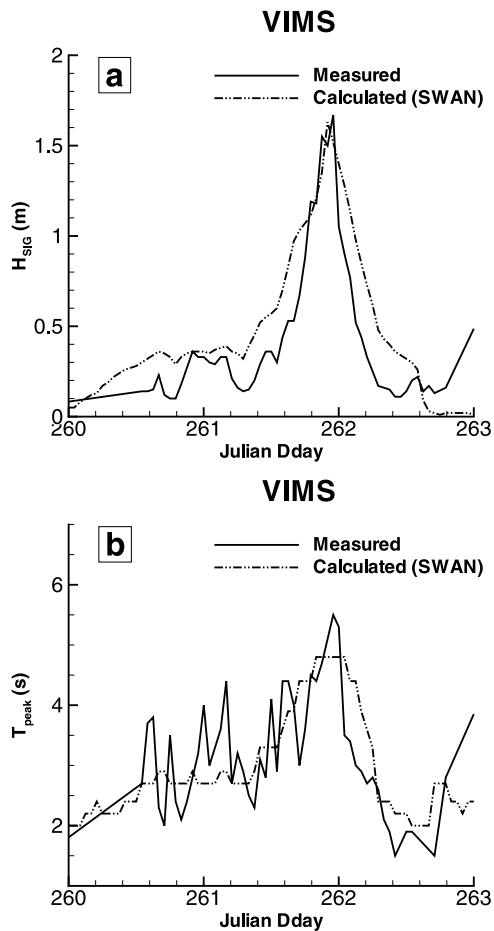


**Figure 8.** Measured versus SWAN simulated wave conditions at the VIMS station.

[38] The area of the computational domain is 134,385 km<sup>2</sup> with a total of 548,240 computational grid cells and an average grid spacing of 500 m. A total of 192,608 (35%) of those computational cells are water cells. The grid covers the entire Chesapeake Bay and all of its river basins including land cells for calculation of flooding and drying. The USGS National Elevation Data set (<http://seamless.usgs.gov/>) data, with a resolution of 1 arc second ( $\sim 30$  m), were interpolated spatially to provide the overland topography for the CH3D grid. The GEODAS bathymetric data were interpolated spatially over the water cells of CH3D grid. Both data sets were converted to the standard NAVD88 vertical datum. The high-resolution USDOT shoreline was utilized to distinguish between land and water. A boundary-fitted curvilinear grid for CH3D was created to fit the complex shoreline and small-scale features, such as inlets and islands. The grid extends far inland to elevation of tens of meters where coastal water could not reach the inland boundaries during Isabel.

[39] For simulation of Isabel over the CH3D domain, water levels along the open boundaries are obtained by combining the surge elevations simulated by the ADCIRC model and tidal constituents (M2, S2, N2, K1, O1, K2, and Q1) provided from the ADCIRC tidal database for the western North Atlantic, Caribbean and Gulf of Mexico. While the ADCIRC tidal database was partially validated

(except nonlinearly generated constituents M4, M6, and STEADY) by Mukai *et al.* [2002], there are some errors associated with the constituents. To reduce the errors associated with the ADCIRC constituents along the open boundaries of the CH3D domain, ADCIRC tidal constituents are compared to tidal constituents calculated from measured data using the IOS tidal analysis program [Foreman, 1977]. Water level data at Duck Pier, North Carolina (on the eastern open boundary), and Beaufort, North Carolina (on the southern open boundary), during a 2 month period, 15 September to 15 November 2003, were used for the IOS program. To improve CH3D simulation of surge and wave during Hurricane Isabel, the ADCIRC tidal constituents along the open boundaries of CH3D were adjusted accordingly.

## 2.5. How Accurate Are ANA, WNA, and WGN Winds?

[40] Accuracy of the wind field plays a major role in affecting the accuracy of the storm surge and wave simulations during hurricanes. In this study, we use the WNA wind provided by NCEP, the WINDGEN (WGN) wind provided through the University of Miami, and the Analytical (ANA) wind based on a relatively simple parametric wind model slightly modified from Holland [1980]. The resolution of the WGN wind is 0.2 degrees and the resolution of the WNA wind is 0.25 degrees, while the ANA wind is calculated at each cell of the model domain without spatial interpolation or extrapolation. Moreover, WGN and WNA winds are available every 3 h, hence temporal interpolation is needed to obtain the instantaneous winds, while ANA wind is calculated at every time step hence no temporal or spatial interpolation is needed. Therefore, the ANA wind is expected to contain more accurate hurricane structure than the WGN or WNA winds.

[41] Figure 4 shows a comparison between measured and simulated wind vectors at four wind stations (Duck Pier, North Carolina; Gloucester Point, Virginia; Cape Lookout, North Carolina; and HPLWS, Maryland) within the computational domain during Isabel. The simulated winds compare quite well with measured wind at the Outer Banks and near the mouth of the Chesapeake Bay. Inside the Chesapeake Bay, the simulated winds are slightly higher than the observed wind at land stations with the ANA winds being more organized, while WNA and WGN winds are less organized owing to spatial and temporal interpolations from the available 3 hourly wind fields. Overall comparison of these three winds over the model domain did not reveal drastic differences, but ANA winds are generally slightly stronger than WGN and WNA winds in open water areas away from land. Unfortunately, not enough wind data from open water wind stations are available for comparison.

## 3. Validation of Hydrodynamic and Wave Simulations

### 3.1. Wave Conditions Along Open Boundaries of CH3D/SWAN Model Domain

[42] Wave conditions along the open boundaries of the SWAN/CH3D model domain during Isabel are obtained from the regional wave model WW3. Figure 5 shows a comparison between WW3 results and measured significant wave height and peak wave period at NDBC buoys 41001

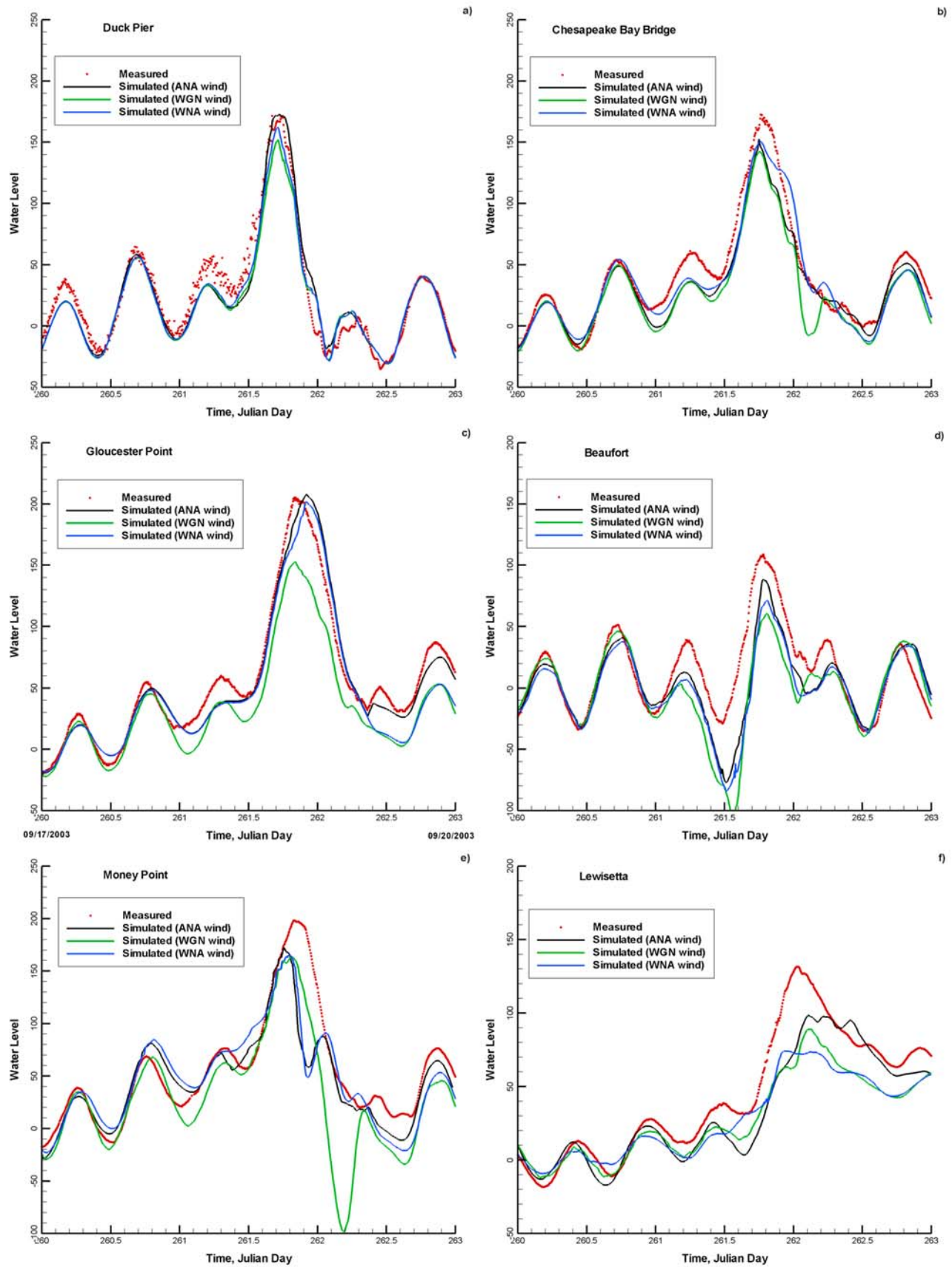


**Figure 9.** Measured and simulated (with current–wave interaction) water levels using CH3D, SWAN, and ANA, WGN, and WNA wind fields.

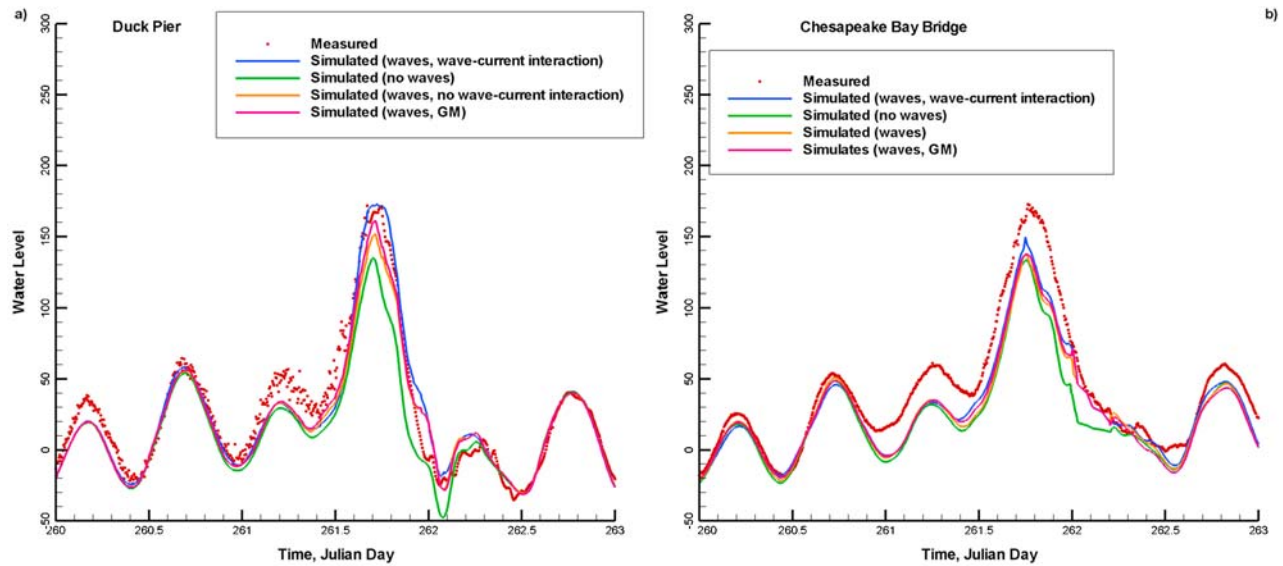


**Figure 10.** Measured and simulated water level at two stations during Isabel using CH3D with various wave-current interaction options, and ANA wind.

and 41002, located a couple of hundred kilometers off the coast of North Carolina, during September 2003. These plots show that the simulated and measured wave parameters are in good agreement, although the significant wave height at 41002 is underestimated just before the wave height peaked owing to Isabel around Julian Day 260.

**3.2. Simulated Versus Measured Wave at Duck and Gloucester**

[43] In the nearshore zone, spatial gradients of radiation stresses produced by breaking waves can create wave setup; that is, a rise in water elevation from the breaker zone to the shoreline. The radiation stresses depend on such wave parameters as wave height, wave period, and wave direction. Depending on the wave condition and the local

bathymetry, wave setup can contribute significantly to the storm surge elevation and affect the local currents. To obtain accurate simulation of wave setup and storm surge, it is essential to have accurate simulation of nearshore wave-fields. We assess the accuracy of simulated wave conditions during Isabel using SWAN and three sets of wave data: two data sets from the Field Research Facilities (FRF) at Duck, North Carolina, and one set from Gloucester Point, Virginia, provided by Virginia Institute of Marine Science (VIMS).

[44] The measured and SWAN simulated wave conditions at the FRF Waverider, approximately 4 km offshore (to be referred to as Duck 630) where the depth is 17 m, are compared. The maximum measured significant wave height at the FRF Waverider buoy during Hurricane Isabel was

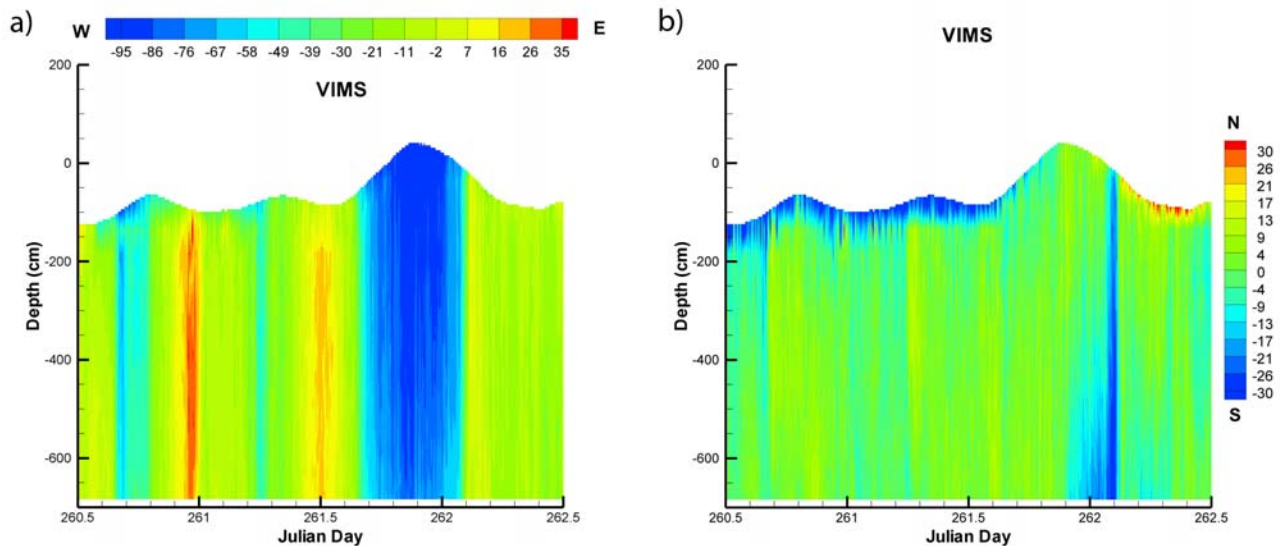


**Figure 11.** Measured (a) east-west and (b) north-south currents at VIMS station.

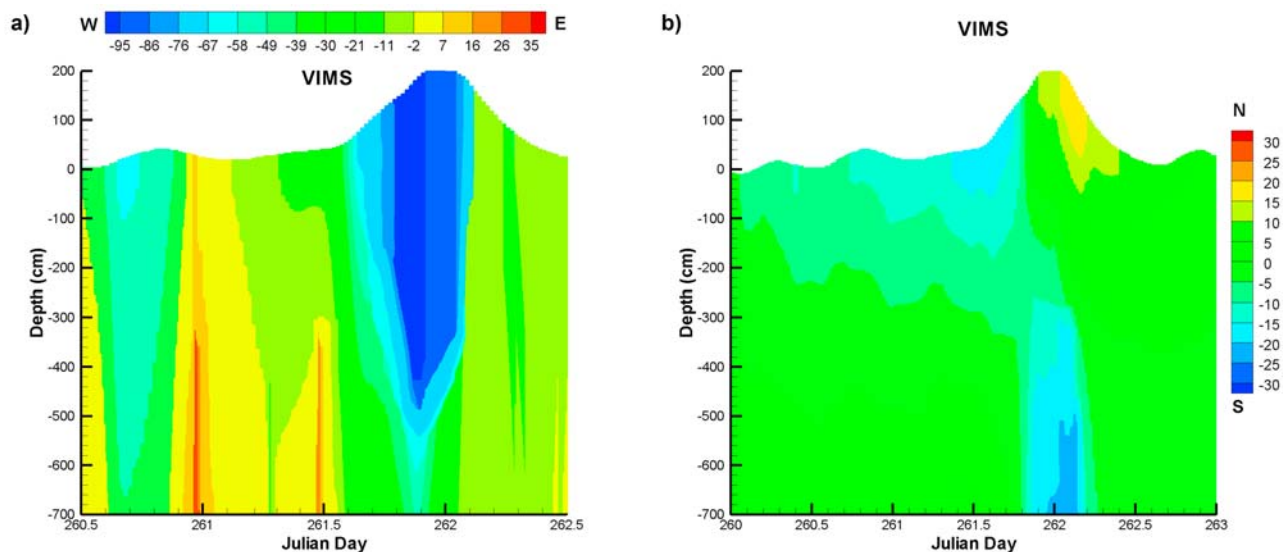


**Figure 12.** Simulated (a) east-west and (b) north-south currents at VIMS station obtained using coupled CH3D/SWAN with a lookup table for wave–current bottom stress and ANA wind field.

8.1 m, while the largest wave (crest to trough) recorded on 18 September at 1911 UT, was 12.1 m. The ratio of the largest wave to local water depth, 0.71, indicates waves were starting to break. The simulated versus measured significant wave height, peak wave period and wave direction are shown in Figure 6. The simulated results presented here are obtained using the WNA wind, since the WGN wind for Isabel was slightly less accurate. The simulated wave height matches well with the measured data with slight underestimation at the peak. There is also a phase lag just before the peak that may be due to swell waves generated outside of the computational domain which could not be properly simulated by the SWAN model. This is because the wave height boundary conditions obtained from

the regional WW3 model are slightly below the measured values right before Hurricane Isabel passed over the area, thus resulting in lower than expected wave setup right before the peak of the storm. Nevertheless, the simulated and measured peak wave height and period values appear to match well.

[45] Figure 7 shows the simulated and measured wave parameters at the end of the FRF Pier approximately 600 m offshore (to be referred to as Duck Pier 625) where the depth is 8.4 m and the maximum measured significant wave height during Hurricane Isabel was 3.7 m. Again, the simulated and measured peak significant wave height and peak wave period compare quite well, although the wave

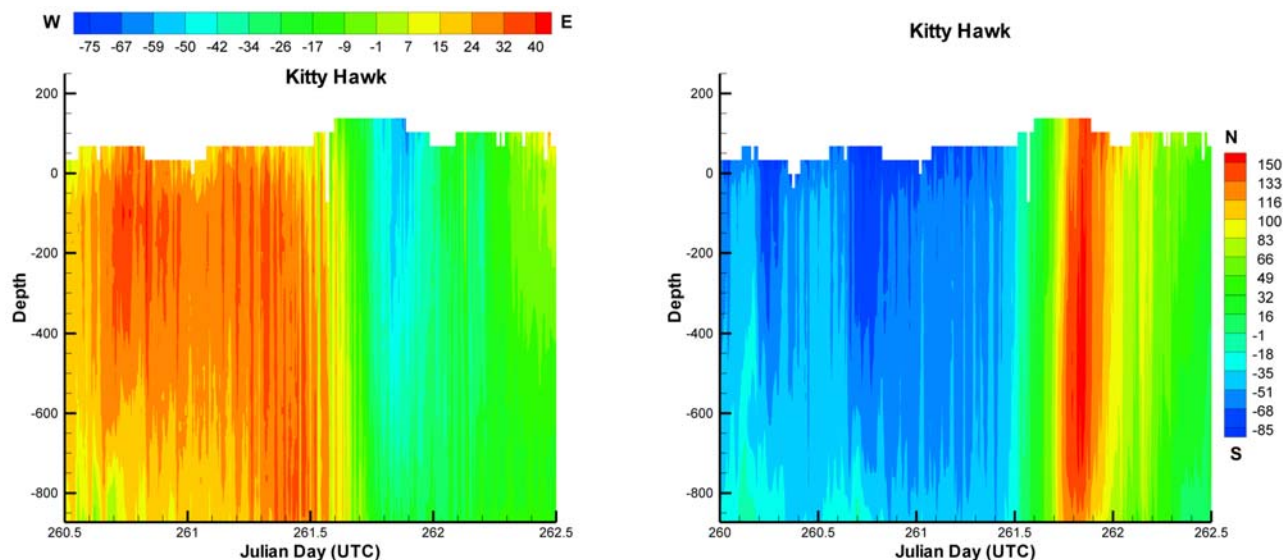


**Figure 13.** (left) Measured onshore-offshore currents and (right) downshore-upshore currents at Kitty Hawk, North Carolina, during Hurricane Isabel.

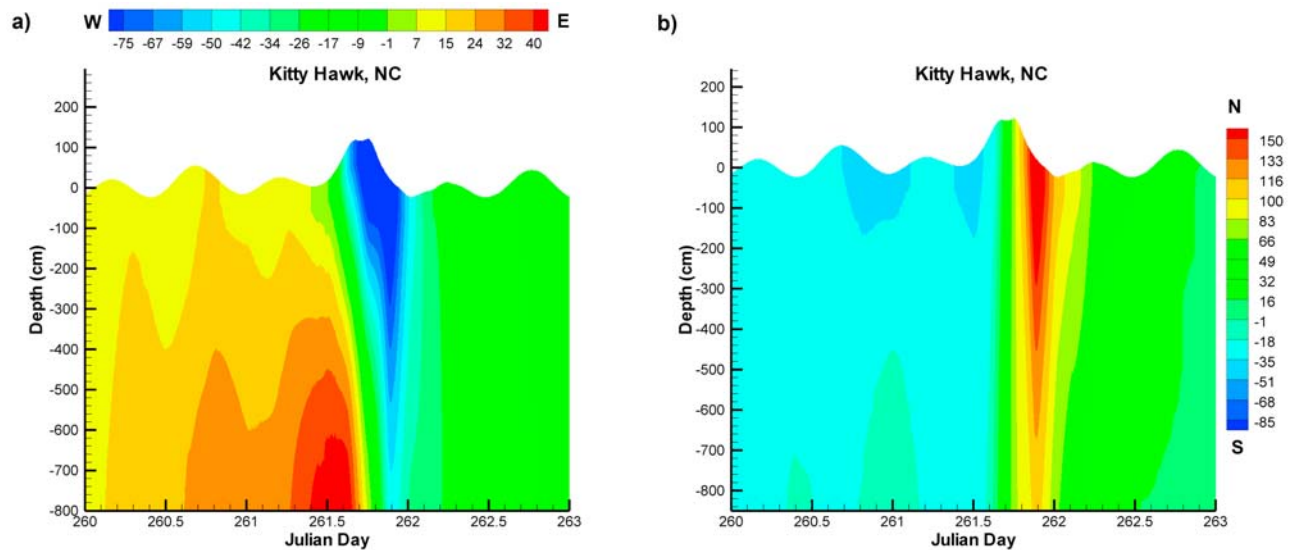


**Figure 14.** (a) Onshore-offshore currents and (b) downshore and upshore currents at Kitty Hawk simulated using CH3D-SSMS with a wave–current bottom stress lookup table and WNA wind.

height was slightly underestimated approximately one day before the peak storm wind arrived.

[46] Waves are quite significant at Gloucester Point, Virginia (referred to as “VIMS,” the data provider), where the depth at the location is around 8.5 m, with a maximum measured significant wave height of 1.7 m. Both the significant wave height and the peak wave period are well simulated, as shown in Figure 8. Errors in wave simulation can be attributed primarily to errors in the open boundary condition provide by WW3, and partially to errors in the WNA wind that often slightly exceeds the measured wind locally. The simulated peak wave period agrees well with the observed.

### 3.3. Validation of Storm Surge Simulations

[47] Several simulations were carried out using ANA/WNA/WGN wind while including or excluding wave effects. Simulated water elevations, using ANA/WNA/WGN wind and including wave effects, are compared with measured water elevations at six stations in Figure 9. Figure 9 shows that simulated water levels obtained with the ANA wind compare the best with observation data. At any particular data station, the response of water level to wind and storm surge depends significantly on the local condition (e.g., any sheltering effect of land or structure). For example, at Gloucester Point, the relatively lower water level owing to the WGN wind was because of the lower southeasterly (parallel to the York River) wind compared to the ANA and WNA winds. The stronger southerly ANA wind did not cause higher water level owing to the narrow river width in the north-south direction. At Money Point, which is at a far upstream station, significant “set down” of water level was caused by the WGN wind which erroneously lined up with the river channel. Such errors in local wind conditions are often created owing to spatial and temporal interpolation from wind fields with relatively coarse spatial and temporal resolutions.

[48] The simulated winds along the Outer Banks and in lower Chesapeake Bay agree well with data and, as a result, the simulated water elevations agree well with measured data. It is noted that the simulated peak water surface elevations match the measured ones well at Duck, Chesapeake Bay Bridge Tunnel, and Gloucester Point. A slight underestimation just before the peak elevation can be observed at all the stations. As pointed out in section 3.2, the simulated wave height before the peak are underestimated owing to the underestimated open boundary wave conditions provided by the WW3 model. This underestimation resulted in lower than expected wave setup right before the peak of the storm. However, wave height at the peak of the storm was accurately simulated, which resulted in adequate contribution of calculated wave setup to the simulated water level at that time.

[49] Figure 10 shows the measured and simulated water level at two stations using ANA wind input and CH3D/SWAN with various wave–current interaction options: no wave effects, no wave–current interaction, with wave effects but different formulas for wave–current bottom stress. It is apparent that the best results are obtained when current–wave interaction is included and bottom stress is included using the lookup table produced by the Sheng-Villaret (SV) model.

### 3.4. Simulated Versus Measured Current Profiles at Gloucester and Kitty Hawk

[50] Measured surface elevation and currents at the VIMS station exhibit periods of the M2 tide as Figure 11a shows significant eastward currents around Julian Day 261 and 261.5. From Julian Day 261.75 to 262.1, the incoming storm surge caused strong westward currents throughout the water column (~8 m). Simulated currents obtained using coupled CH3D/SWAN and wave–current interaction bottom stress lookup table and ANA wind input show similar results in Figure 12. Significant eastward currents are found at Julian Day 261 and 261.5, while strong westward

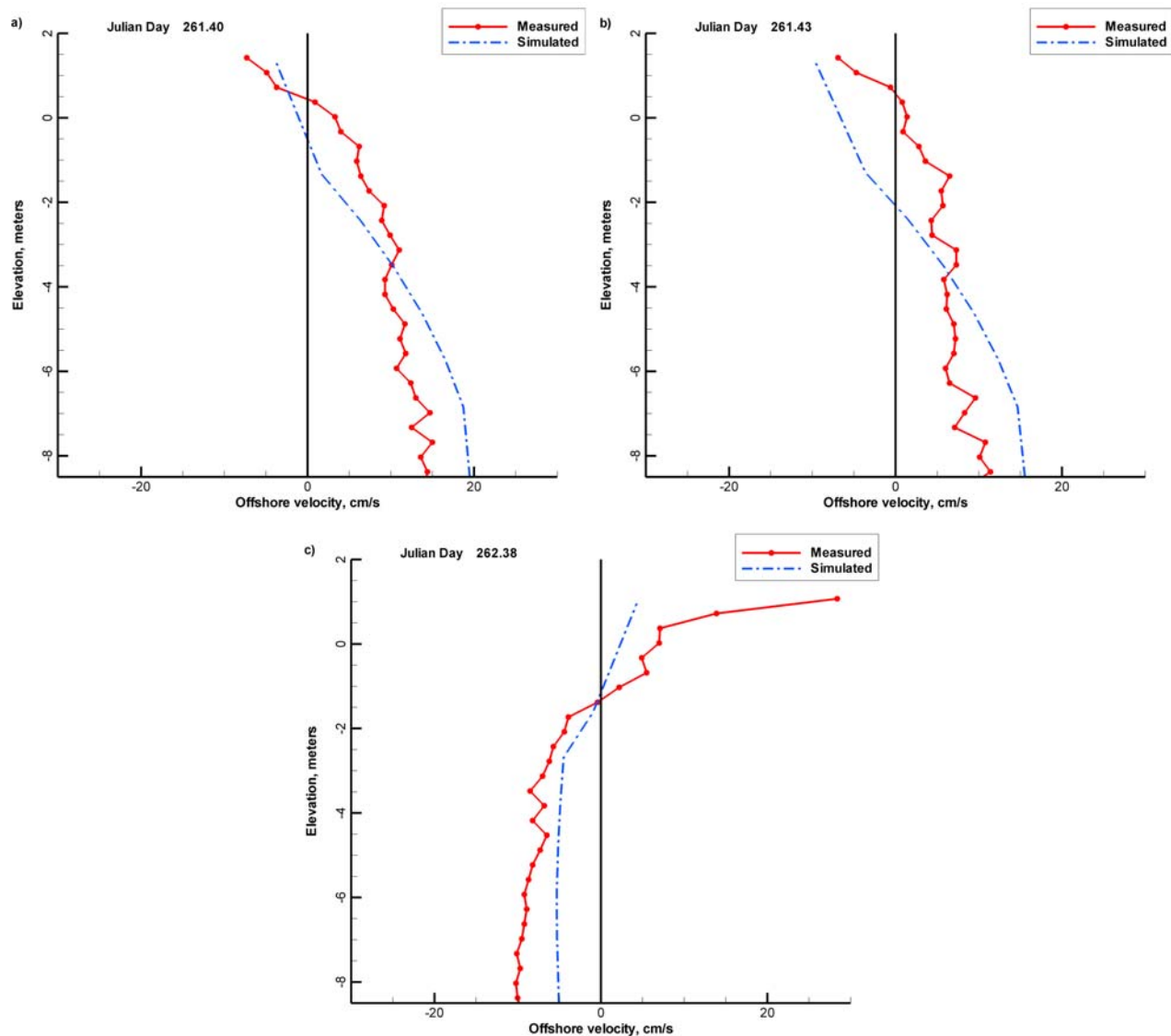


**Figure 15.** Measured and simulated onshore-offshore currents at Kitty Hawk during Isabel.

currents are found during Julian Day 261.75 and 262.1. Both measured and simulated north-south currents show flow reversal between the surface and bottom waters between Julian Day 261.9 and 262.1.

[51] Measured and simulated currents at Kitty Hawk are also presented here. Figure 13 shows the measured onshore-offshore and downshore-upshore currents at Kitty Hawk, while Figure 14 (with WNA wind) shows the simulated currents. Prior to the arrival of hurricane wind around Julian Day 261.7, data showed strong southeastward (offshore and downshore) currents which are apparently wind driven but are underestimated by the model owing to lower simulated wind. During Julian Day 261.7 and 261.9, peak easterly and southeasterly wind caused strong currents in onshore and upshore directions and both measured and simulated currents show a vertical structure with onshore flow near the surface and offshore flow near the bottom. Results (not shown) obtained using ANA wind, which is weaker than WNA wind at Duck, are slightly worse. While the simulated currents do not agree completely with the observed currents,

the results are encouraging considering the relatively coarse grid resolution (eight vertical layers and four to six horizontal cells between the Kitty Hawk station and the shoreline) and uncertainty in bathymetry in the vicinity. Measured and simulated onshore-offshore velocity at Kitty Hawk at the peak of storm surge exhibits a two-layer flow structure as shown in Figure 15. This two-layer flow structure is apparently caused by hurricane force wind as well as breaking hurricane wave. Before and after the peak storm surge, this two-layer flow structure did not exist.

## 4. Discussion

### 4.1. Evolution of Storm Surge During Isabel

[52] Five snapshots of instantaneous water level in the Chesapeake Bay and Outer Banks are shown in Figures 16a–16e to illustrate the evolution of storm surge during Isabel on the basis of model simulations using ANA wind. For clarity, water levels over land areas are not shown. At 1330 UT on 18 September (Julian Day 261), as shown in Figure 16a, a

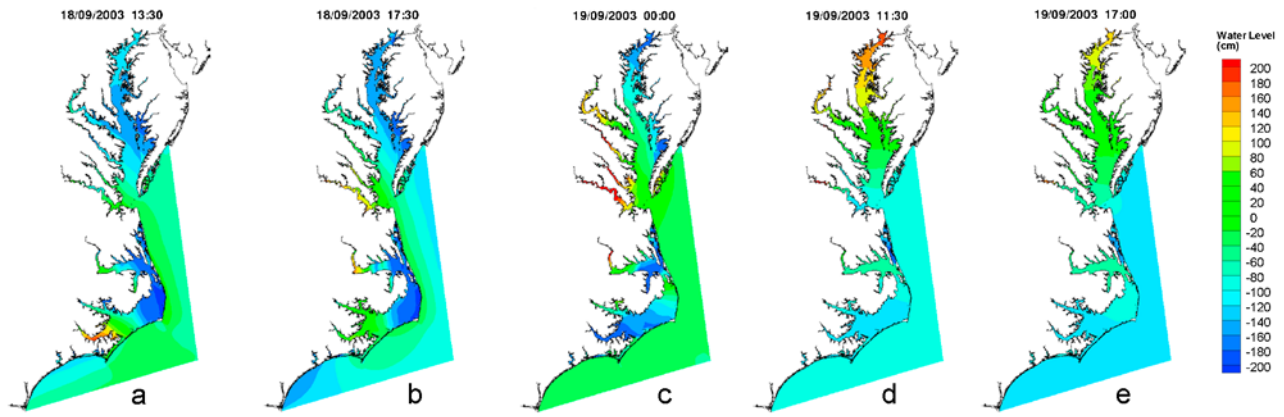


**Figure 16.** Snapshots of water level at five instants in study area during Isabel.

few hours before Isabel made landfall, wind starts to increase and switch from northeasterly to easterly, and peak water level is found inside the Pamlico Sound. At 1730 UT, as shown in Figure 16b, Isabel landfalls to the east of Cape Outlook and Beaufort, and wind starts to switch from easterly to southeasterly. As shown in Figure 9, water elevations at Duck, Beaufort, Chesapeake Bay Bridge, and Gloucester all peaked around this time when tide at Duck also peaked. Between 1730 and 2400 UT (Figure 16c),

strong southeasterly wind pushes the surge and high water into Chesapeake Bay, leading to high water level in southern Chesapeake Bay, James River, and York River. From 2400 UT on, southerly wind persists for more than 12 h in most of the Chesapeake Bay, and generates a significant south-to-north setup of water level, as shown in Figure 16d (1130 on 19 September) and Figure 16e (1700 UT on 19 September).

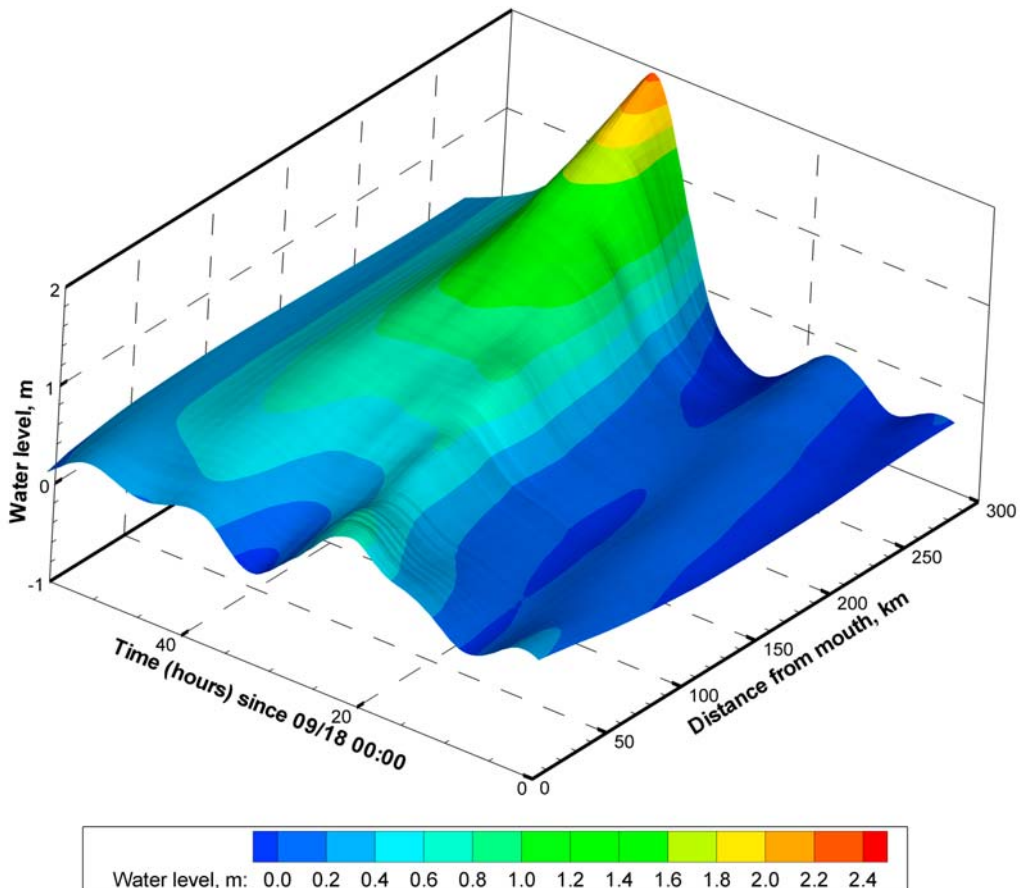


**Figure 17.** Evolution of water level along the major axis during Isabel.

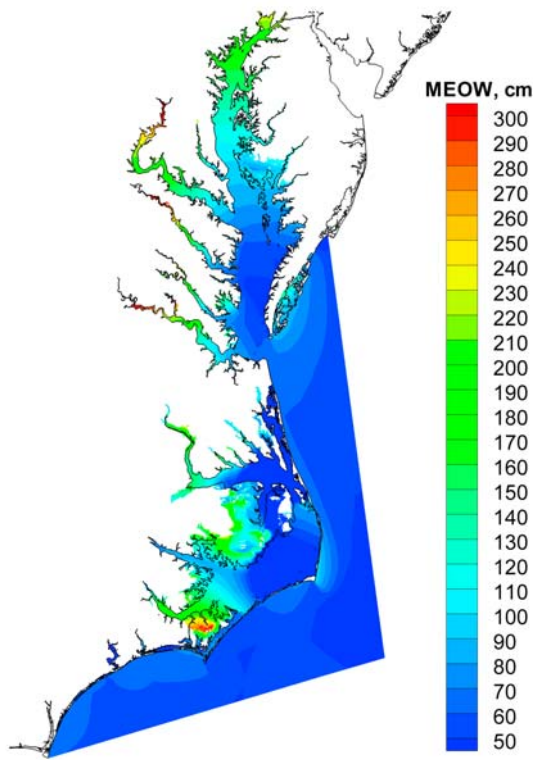


**Figure 18.** Maximum envelope of water (MEOW) simulated using WGN wind.

[53] To illustrate the more detailed evolution of water level during Isabel, the simulated water level along the major axis of Chesapeake Bay (Figure 2) is plotted as a function of space and time in Figure 17. The result as shown

in Figure 17 compares qualitatively well with that produced by *Shen et al.* [2006] using a different storm surge model but without a wave model. Results obtained with WNA and WGN winds are also similar with slight differences in peak elevation and timing.

**4.2. Simulated Maximum Envelope of Water**

[54] Maximum envelope of water (MEOW) is the maximum simulated water elevations (including tide, surge and wave setup) throughout a model simulation. Figure 18 shows the MEOW in the Outer Banks and Chesapeake Bay during Isabel, calculated using the WGN wind. The MEOW simulated using ANA wind shows slightly higher inundation in the land area owing to generally slightly stronger ANA wind inside Chesapeake Bay.

**4.3. Effect of Wave on MEOW**

[55] To examine the effect of wave on the maximum water level during Isabel, we calculate the maximum water level owing to wave effect by subtracting the MEOW owing to wind and tide from the MEOW owing to wind, tide, and wave. The resulting maximum envelope of water gives the MEOW owing to wave effect only (MEOWW). Figure 19a shows the maximum envelope of significant wave height (MESWH) during Isabel, while Figure 19b shows the maximum envelope of water owing to wave (MEOWW). As shown in Figures 19a and 19b, high wave is found in coastal region as well as inside Chesapeake Bay, and the effect of wave on maximum water elevation is very significant, reaching 30–100 cm within most of the Chesapeake Bay and the major rivers. High waves along the Cape Hatteras National Seashore, in combination with the high surge, most likely resulted in inundation and breaching of the barrier island during Isabel.

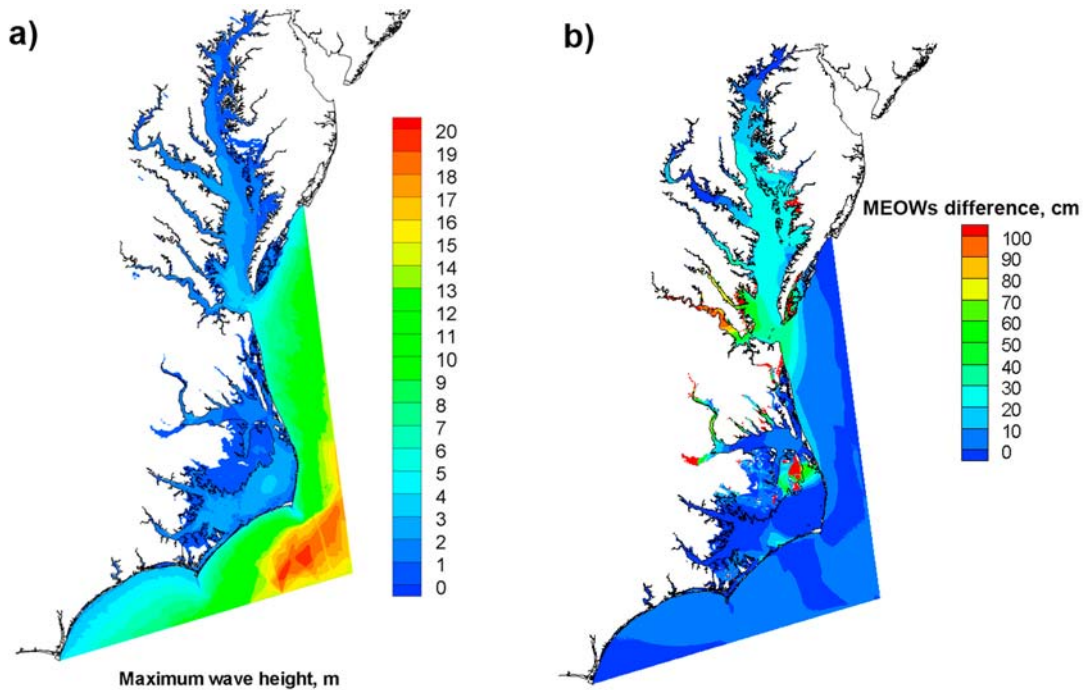


**Figure 19.** (a) Maximum envelope of significant wave height simulated using WNA wind. (b) Maximum envelope of water due to wave simulated using WNA wind.

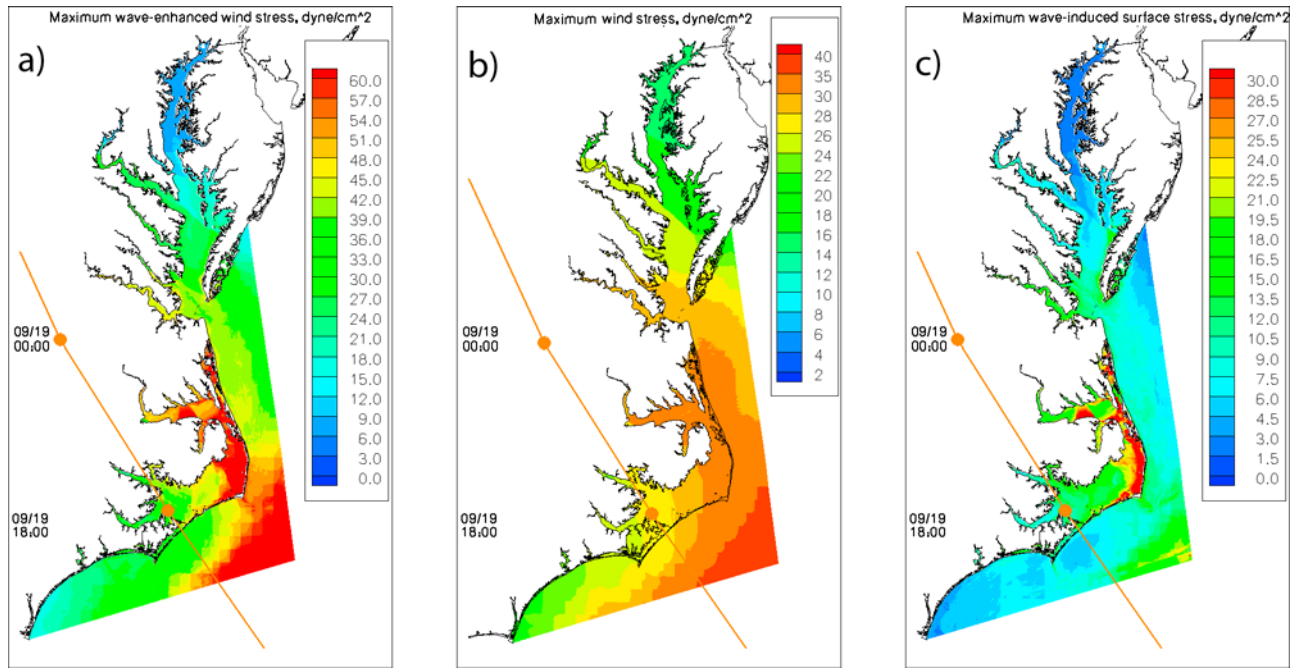


**Figure 20.** (a) Maximum wave-enhanced wind stress, (b) maximum wind stress, and (c) maximum wave-induced surface stress during Hurricane Isabel.

[56] It is interesting to point out that while wave height near the mouth of Chesapeake Bay and along the north shore of North Carolina is comparable to that along the south shore of North Carolina, wave-induced water elevation is much lower along the south shore because wind direction during Isabel was mostly parallel to the shore hence did not generate much wave setup. Wave-induced water level is quite significant inside the Chesapeake Bay, because of favorable wind direction (particularly inside James River) and significance of wave-induced wind stress. Wave-induced water level along the north shore of North Carolina, including the Duck area, is significant because of quite significant radiation stress gradients perpendicular to the shoreline associated with the onshore-directed wind of Isabel.

**4.4. Effect of Wave on Wind Stress and Horizontal Momentum**

[57] We show the maximum wave-enhanced wind stress, maximum wind stress (without wave effect), and maximum wave-induced surface stress in the model domain generated by the WNA wind during Hurricane Isabel in Figures 20a, 20b, and 20c, respectively. The wave-induced surface stress shown in Figure 20c is quite significant particularly inside the southern Chesapeake Bay and Pamlico Sound, which explains the significant wave-induced water level there shown in Figure 19b. Therefore, inside the southern Chesapeake Bay and Pamlico Sound, wave-induced water level increases mainly owing to the increased wave-induced surface stress, while the wave-induced radiation stress gradient is negligible there as shown in Figure 21. Significant radiation stress gradients are found along the north shore of North Carolina including Duck, plus the deeper water off the south shore of North Carolina. The significant

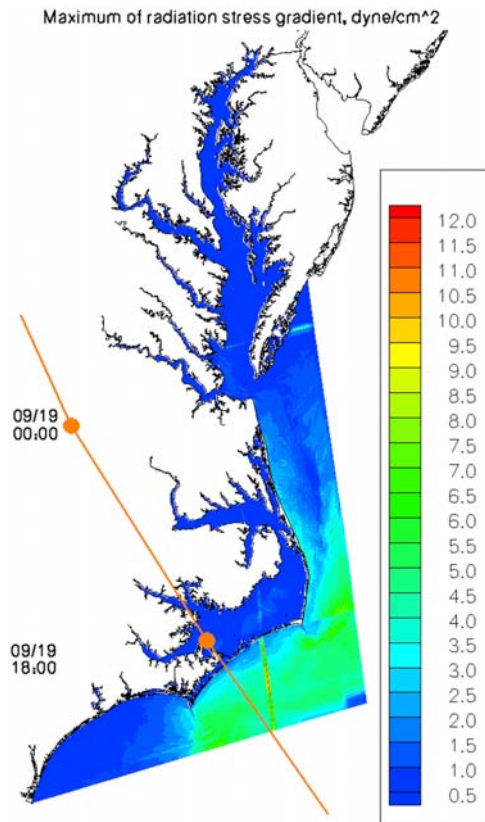


**Figure 21.** Maximum radiation stress gradients during Isabel.

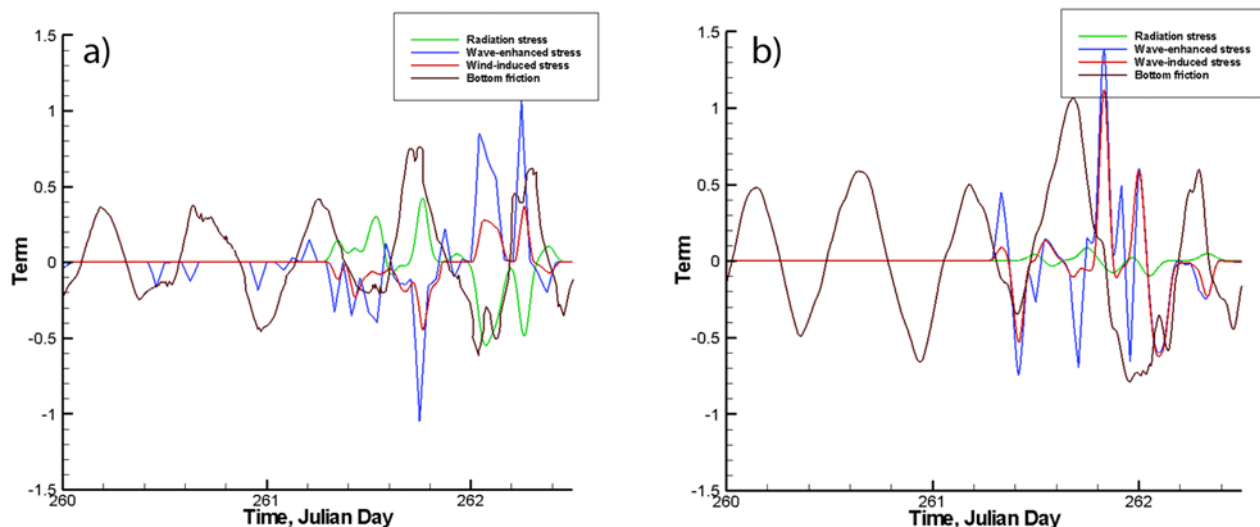


**Figure 22.** (a) Evolution of dimensionless wave-enhanced surface stress, wave-induced surface stress, radiation stress gradient, and wave-enhanced bottom stress in onshore-offshore direction at a coastal station near Duck, North Carolina, during Hurricane Isabel. (b) Evolution of dimensionless wave-enhanced surface stress, wave-induced surface stress, radiation stress gradient, and wave-enhanced bottom stress in the north-south direction at a Chesapeake Bay station during Hurricane Isabel.

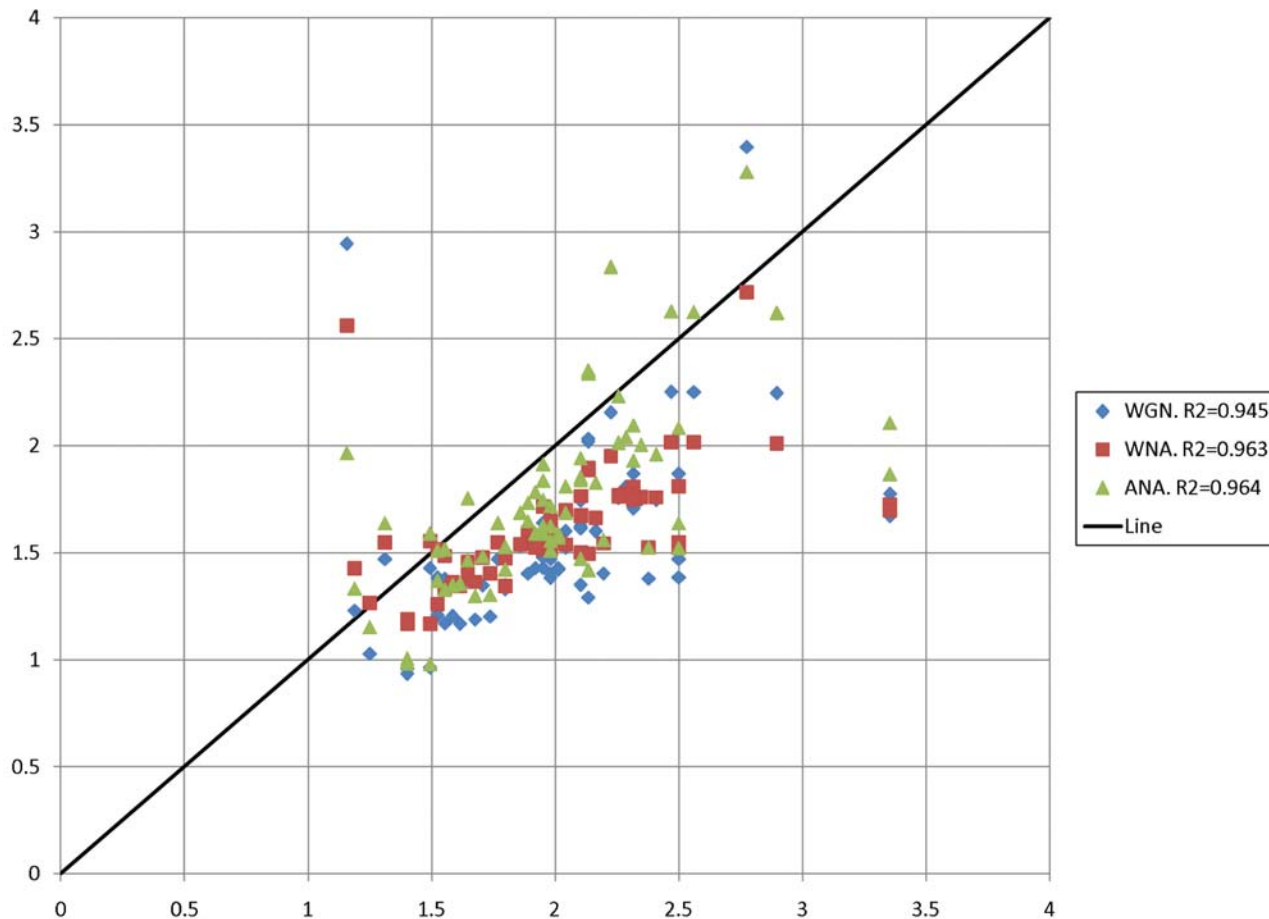


**Figure 23.** Simulated versus measured HWMs.



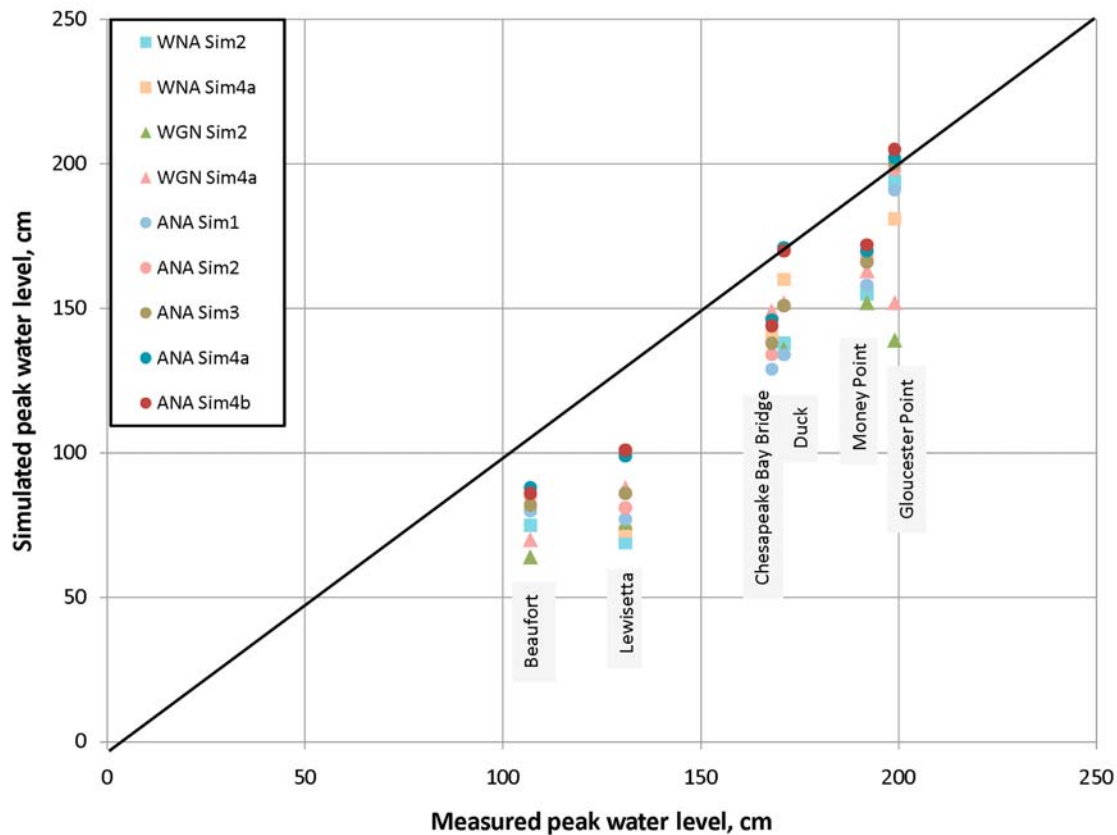


**Figure 24.** Comparison between simulated and measured water level at six stations during Isabel.

shows that wave-induced surface stress clearly dominates the radiation stress gradient at the Chesapeake Bay station.

#### 4.5. Accuracy of Simulated High Water Marks

[59] High water marks (HWMs) at numerous stations shown in Figure 2 are used to compare with simulated HWMs obtained using WGN, WNA, and ANA winds. As shown in Figure 23, HWMs simulated using the ANA wind agree the best with the measured ones, while HWMs produced using WGN and WNA winds are generally slightly underestimated.

#### 4.6. How Sensitive Is Simulated Storm Surge Elevation to Various Model Features?

[60] In order to assess the effects of various factors on simulated storm surge throughout the model domain during Isabel, several simulations were made. Table 2 specifies the five specific model features included in five simulation categories. Table 3 shows the RMS error of simulated water elevation at six stations during Isabel. Errors of peak values (measured peak elevation minus simulated peak elevation) and “timing” errors (the time when measured peak elevation occurred minus the time when simulated peak elevation occurred) are also shown. A separate column displays the errors associated with the “pure” tide simulation, which only included tidal forcing at the open boundaries.

[61] On the basis of this error analysis, particularly the average RMS errors and average absolute errors at the peak water elevation, it can be concluded that the ANA wind produced generally more accurate water level at all stations.

This is consistent with the earlier analysis which showed that WNA and WGN winds, because of spatial and temporal interpolation from rather sparse and coarse-resolution wind fields, are somewhat less accurate than the ANA wind inside the Chesapeake Bay. Temporal interpolation of sparse wind fields, particularly near landfall time, tends to distort hurricane structures and generate artificially lower wind speed and erroneous direction. However, ANA wind is generated at every grid cell every time step, hence retains the hurricane structure throughout the simulation. The accuracy of the simulated water elevation, which includes tide, depends on the accurate simulation of tide which is accurate across the Outer Banks up to the mouth of the Chesapeake Bay, with the average RMS error of approximately 4 cm. Inside the bay, the accuracy of the simulated tide worsens, with the average RMS error increasing to 6 cm. So did the accuracy of the simulated water elevation, which was also accompanied with the worse accuracy of the WNA wind inside the Chesapeake Bay as opposed to that over the Outer Banks. In general, ANA wind produced more accurate water elevation and inundation (as measured by HWMs) inside the Chesapeake Bay, as shown in Figures 23 and 24.

[62] On the basis of Table 2 and Figure 24, simulation 4 produces the best overall water level agreement with slightly smaller RMS errors and better comparison with measured water surface elevation at its peak. In the Outer Banks region, the inclusion of WNA wind led to good simulated water elevation. After Isabel made landfall, the simulated water elevation at Beaufort is not very good because the

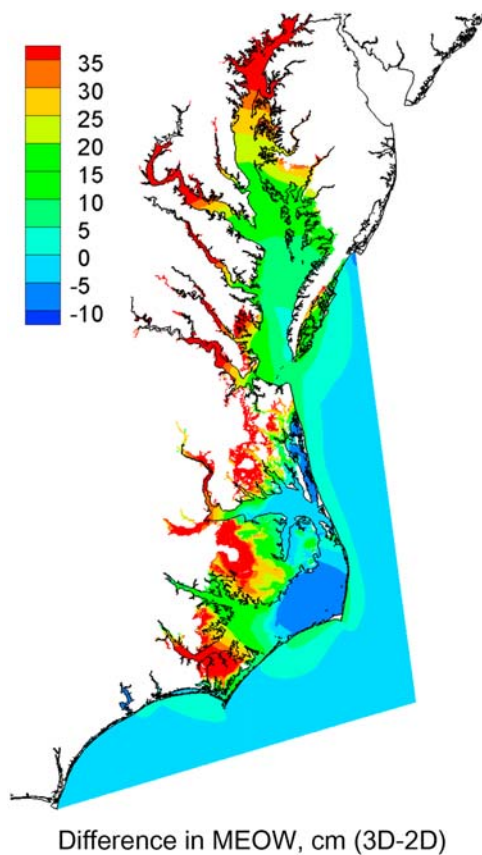


**Figure 25.** Difference between the maximum envelope of water during Isabel obtained by the 2- and 3-D simulations using ANA wind.

effect of land dissipation on wind is not included. Inside Chesapeake Bay, the WNA wind (based on extrapolation of coastal wind) gives less accurate results. WGN wind, which is slightly more accurate than the extrapolated WNA wind inside Chesapeake Bay, provided a slightly more accurate water elevation prediction. The ANA wind gives generally more accurate water elevation results over the entire model domain. However, the effect of land dissipation on hurricane wind [e.g., *IPET*, 2006] has not been included in this simple analytical wind model.

#### 4.7. Three-Dimensional Effects on Simulated Storm Surge, Wave, and Inundation

[63] The Maximum Envelope of Water (MEOW) results during Isabel obtained by the 2- and 3-D simulations are compared and the difference between the 3- and 2-D water level is shown in Figure 25. Both models include the wave effects; the 2-D simulation was based on coupled SWAN and the 2-D version of CH3D, the 3-D simulation is based on coupled SWAN with the 3-D version of CH3D. While the radiation stress formulation is the same for both the 2- and 3-D simulations, the wave–current bottom stress formulation is different. In the 2-D simulation, wave-induced bottom stress is kinematically combined with current-induced bottom stress to produce the total bottom stress averaged over the wave cycle [Sheng and Lick, 1979; Bijker 1966, 1986]. The 3-D bottom stress is obtained from the

lookup table which is based on the results of nonlinearly coupled wave turbulence model of Sheng and Villaret [1989]. Therefore the wave–current bottom stress in the 2-D simulation tends to be higher than that in the 3-D simulation. This explains the slightly higher maximum water elevation in the 3-D results throughout most of the model domain, as shown in Figure 25. Using the 2- or 3-D versions of CH3D only made very slight difference (no more than 5 cm) on the maximum significant wave height throughout the model domain.

## 5. Conclusions

[64] An integrated modeling system CH3D-SSMS has been used to simulate the storm surge, wave effect, and inundation in the Outer Banks and Chesapeake Bay area during Hurricane Isabel. Model results are found to reasonably reproduce the observed wind, storm surge, wave, currents, and inundation in the study area. The three wind fields (ANA, WGN, and WNA) all give reasonable wind at the coastal stations prior to Isabel landfall, while the ANA wind is found to be generally slightly more accurate than the WGN and WNA winds in the Chesapeake Bay region after the landfall. Producing accurate over-the-land wind after hurricane landfall remains a major challenge.

[65] The most notable results are that the model simulated the significant effects of waves on storm surge, currents, and inundation. Among the three resolved processes which represent wave effects, wave-induced radiation stress (outside and inside the estuaries) and wave-induced surface stress (outside and inside the estuaries) are the dominant ones, while wave-induced bottom stress is of secondary importance. The best results are obtained when SWAN is coupled to the 3-D version of CH3D, with all three wave effects included. The inclusion of radiation stress improved the computed storm surge by up to 18%, with the most significant improvement at Beaufort and Duck where high breaking waves caused significant setup. Including wave-induced surface stress improved the calculated storm surge by up to 16%, while including wave-induced bottom friction led to up to 5% reduction in the peak storm surge level. Wave-enhanced bottom stress in the coupled CH3D-SWAN is higher when the 2-D version of CH3D is used.

[66] Observation data and model simulation yielded the following interesting results. Maximum water elevation in the study area reached 2.5 m during Isabel, while maximum wave height reached  $\sim 20$  m offshore and up to 4 m inside the Chesapeake Bay. Maximum wave-induced water level reached 1 m inside the Chesapeake Bay. Significant waves reached 3.5 m and 16 s at the Duck Pier, and 1.6 m and 5 s at Gloucester, Virginia. Offshore waves led to breaking and large wave setup, which accounted for  $\sim 36$  cm or 20% of the peak surge elevation of 1.71 m at Duck. Inside the Chesapeake Bay, wave setup accounts for 5–10% of observed peak surge elevation. At Kitty Hawk, a two-layer flow (with onshore surface current and offshore current underneath) is found during the peak of storm surge owing to combined effects of wind and wave breaking. Currents around 1 m/s were found at Gloucester.

[67] Although water levels simulated by 2- and 3-D models do not differ significantly at selected stations, the 3-D results show noticeably more inundation. The 3-D

model is necessary for accurate simulation of observed currents at Gloucester and Kitty Hawk that are driven by wind, tide, and radiation stress. The 3-D model also allows inclusion of more robust wave–current interaction processes, including the radiation stress formulation and wave-enhanced bottom stress. The use of the 3-D model and a lookup table provides a novel method for calculating wave-enhanced bottom stress. Further model validation can be conducted if high-resolution field data of wave and turbulence within the bottom boundary layer and the surface layer in the surf zone become available. The modeling system can be used as a framework for testing newly developed current–wave interaction model [e.g., Mellor, 2008], or wave model. Additional insight on the wave processes can be gained by comparing simulated and measured directional wave spectra at data stations. Although the stationary SWAN produced reasonably accurate wave simulation for the Isabel simulation, its application to a faster moving storm needs to be further investigated.

## Appendix A: Equations and Boundary Conditions of the Coastal Surge Model CH3D

### A1. Equations of the Coastal Surge Model CH3D

[68] In Cartesian coordinate system, the governing equations for water continuity, X momentum, and Y momentum equations are:

$$\frac{\partial u}{\partial x} + \frac{\partial v}{\partial y} + \frac{\partial w}{\partial z} = 0 \quad (\text{A1})$$

$$\begin{aligned} \frac{\partial u}{\partial t} + \frac{\partial uu}{\partial x} + \frac{\partial uv}{\partial y} + \frac{\partial uw}{\partial z} + \frac{1}{\rho_w} \frac{\partial S_{xx}}{\partial x} + \frac{1}{\rho_w} \frac{\partial S_{xy}}{\partial y} \\ = -g \frac{\partial \zeta}{\partial x} - \frac{1}{\rho_w} \frac{\partial P_a}{\partial x} + f v + A_H \left( \frac{\partial^2 u}{\partial x^2} + \frac{\partial^2 u}{\partial y^2} \right) + \frac{\partial}{\partial z} \left( A_V \frac{\partial u}{\partial z} \right) \end{aligned} \quad (\text{A2})$$

$$\begin{aligned} \frac{\partial v}{\partial t} + \frac{\partial uv}{\partial x} + \frac{\partial vv}{\partial y} + \frac{\partial vw}{\partial z} + \frac{1}{\rho_w} \frac{\partial S_{yx}}{\partial x} + \frac{1}{\rho_w} \frac{\partial S_{yy}}{\partial y} \\ = -g \frac{\partial \zeta}{\partial y} - \frac{1}{\rho_w} \frac{\partial P_a}{\partial y} - f u + A_H \left( \frac{\partial^2 v}{\partial x^2} + \frac{\partial^2 v}{\partial y^2} \right) + \frac{\partial}{\partial z} \left( A_V \frac{\partial v}{\partial z} \right) \end{aligned} \quad (\text{A3})$$

where  $u(x; y; z; t)$ ,  $v(x; y; z; t)$ , and  $w(x; y; z; t)$  are the velocity vector components in  $x$ ,  $y$ , and  $z$  coordinate directions, respectively;  $t$  is time;  $\zeta(x; y; t)$  is the free surface elevation;  $g$  is the acceleration of gravity;  $A_H$  and  $A_V$  are the horizontal and vertical turbulent eddy coefficients, respectively;  $S_{xx}$ ,  $S_{xy}$ ,  $S_{yy}$  are radiation stresses,  $P_a$  is atmospheric pressure and  $f$  is the Coriolis parameter.  $A_V$  is calculated by the vertical turbulence model described in the work of Sheng and Villaret [1989], and  $A_H$  by a Smagorinsky-type formula.

[69] Following Sheng [1987, 1990], the nondimensional form of above equations in curvilinear, boundary-fitted grid system can be written as:

$$\frac{\partial \zeta}{\partial t} + \frac{\beta}{\sqrt{g_0}} \left[ \frac{\partial}{\partial \xi} (\sqrt{g_0} Hu) + \frac{\partial}{\partial \eta} (\sqrt{g_0} Hv) \right] + \beta \frac{\partial H \omega}{\partial \sigma} = 0 \quad (\text{A4})$$

$$\begin{aligned} \frac{1}{H} \frac{\partial Hu}{\partial t} = & - \left( g^{11} \frac{\partial \zeta}{\partial \xi} + g^{12} \frac{\partial \zeta}{\partial \eta} \right) + \left( g^{11} \frac{\partial P}{\partial \xi} + g^{12} \frac{\partial P}{\partial \eta} \right) \\ & + \left( \frac{g_{12}}{\sqrt{g_0}} u + \frac{g_{22}}{\sqrt{g_0}} v \right) - \frac{R_0}{g_0} \left\{ x_\eta \left[ \frac{\partial}{\partial \xi} (y_\xi \sqrt{g_0} S_{\xi\xi} + y_\eta \sqrt{g_0} S_{\xi\eta}) \right] \right. \\ & + \frac{\partial}{\partial \eta} (y_\xi \sqrt{g_0} S_{\xi\eta} + y_\eta \sqrt{g_0} S_{\eta\eta}) \left. \right\} - y_\eta \left[ \frac{\partial}{\partial \xi} (x_\xi \sqrt{g_0} S_{\xi\xi} + x_\eta \sqrt{g_0} S_{\xi\eta}) \right. \\ & + \frac{\partial}{\partial \eta} (x_\xi \sqrt{g_0} S_{\xi\eta} + x_\eta \sqrt{g_0} S_{\eta\eta}) \left. \right\} - \frac{R_0}{g_0 H} \left\{ x_\eta \left[ \frac{\partial}{\partial \xi} (y_\xi \sqrt{g_0} Huu \right. \right. \\ & + y_\eta \sqrt{g_0} Huv) + \frac{\partial}{\partial \eta} (y_\xi \sqrt{g_0} Huv + y_\eta \sqrt{g_0} Hvv) \left. \right] \\ & - y_\eta \left[ \frac{\partial}{\partial \xi} (x_\xi \sqrt{g_0} Huu + x_\eta \sqrt{g_0} Huv) \right. \\ & + \frac{\partial}{\partial \eta} (x_\xi \sqrt{g_0} Huv + x_\eta \sqrt{g_0} Hvv) \left. \right] - g_0 \frac{\partial H \omega}{\partial \sigma} \left. \right\} \\ & + \frac{E_v}{H^2} \frac{\partial}{\partial \sigma} \left( A_V \frac{\partial u}{\partial \sigma} \right) + E_H A_H (\text{Horizontal Diffusion of } u) \\ & - \frac{R_0}{F_r^2} \left[ H \int_\sigma^0 \left( g^{11} \frac{\partial \rho}{\partial \xi} + g^{12} \frac{\partial \rho}{\partial \eta} \right) d\sigma \right. \\ & \left. + \left( g^{11} \frac{\partial H}{\partial \xi} + g^{12} \frac{\partial H}{\partial \eta} \right) \left( \int_\sigma^0 \rho d\sigma + \sigma \rho \right) \right] \end{aligned} \quad (\text{A5})$$

$$\begin{aligned} \frac{1}{H} \frac{\partial Hv}{\partial t} = & - \left( g^{21} \frac{\partial \zeta}{\partial \xi} + g^{22} \frac{\partial \zeta}{\partial \eta} \right) - \left( g^{21} \frac{\partial P}{\partial \xi} + g^{22} \frac{\partial P}{\partial \eta} \right) \\ & - \left( \frac{g_{11}}{\sqrt{g_0}} u + \frac{g_{21}}{\sqrt{g_0}} v \right) - \frac{R_0}{g_0} \left\{ x_\xi \left[ \frac{\partial}{\partial \xi} (y_\xi \sqrt{g_0} S_{\eta\xi} + y_\eta \sqrt{g_0} S_{\eta\eta}) \right] \right. \\ & + \frac{\partial}{\partial \eta} (y_\xi \sqrt{g_0} S_{\eta\xi} + y_\eta \sqrt{g_0} S_{\eta\eta}) \left. \right\} - y_\eta \left[ \frac{\partial}{\partial \xi} (x_\xi \sqrt{g_0} S_{\xi\xi} + x_\eta \sqrt{g_0} S_{\xi\eta}) \right. \\ & + \frac{\partial}{\partial \eta} (x_\xi \sqrt{g_0} S_{\xi\eta} + x_\eta \sqrt{g_0} S_{\eta\eta}) \left. \right\} - \frac{R_0}{g_0 H} \left\{ x_\xi \left[ \frac{\partial}{\partial \xi} (y_\xi \sqrt{g_0} Huv \right. \right. \\ & + y_\eta \sqrt{g_0} Hvv) + \frac{\partial}{\partial \eta} (y_\xi \sqrt{g_0} Huv + y_\eta \sqrt{g_0} Hvv) \left. \right] \\ & - y_\eta \left[ \frac{\partial}{\partial \xi} (x_\xi \sqrt{g_0} Huu + x_\eta \sqrt{g_0} Huv) + \frac{\partial}{\partial \eta} (x_\xi \sqrt{g_0} Huv + x_\eta \sqrt{g_0} Hvv) \right] \\ & - g_0 \frac{\partial H \omega}{\partial \sigma} \left. \right\} + \frac{E_v}{H^2} \frac{\partial}{\partial \sigma} \left( A_V \frac{\partial v}{\partial \sigma} \right) + E_H A_H (\text{Horizontal Diffusion of } v) \\ & - \frac{R_0}{F_r^2} \left[ H \int_\sigma^0 \left( g^{21} \frac{\partial \rho}{\partial \xi} + g^{22} \frac{\partial \rho}{\partial \eta} \right) d\sigma + \left( g^{21} \frac{\partial H}{\partial \xi} + g^{22} \frac{\partial H}{\partial \eta} \right) \right. \\ & \left. \cdot \left( \int_\sigma^0 \rho d\sigma + \sigma \rho \right) \right] \end{aligned} \quad (\text{A6})$$

where

- $\xi, \eta$  and  $\sigma$  are the transformed coordinates;
- $u, v, w$  are nondimensional contravariant velocities in curvilinear grid  $(\xi, \eta, \sigma)$ .
- $\sqrt{g_0}$  is the Jacobian of horizontal transformation;
- $g^{11}, g^{22}, g_{11}, g_{12}, g_{22}$  are the metric coefficients of coordinate transformations;
- $\beta$  is nondimensional parameter;
- $\zeta$  is water level;

[70] It can be shown that the wave-averaged equations (A4)–(A6) are valid for two regions: the region between the free surface (mean sea level) and the wave trough, as well as

the region between the wave trough and the bottom. In the region above the wave trough, the wave-averaged horizontal currents include the mean currents and the Stokes drift, while the radiation stress includes the vertically uniform radiation stress according to *Longuet-Higgins and Stewart* [1964] plus that owing to the surface roller [*Svendsen, 1984; Haas and Svendsen, 2000*]. Below the wave trough, the Stokes drift is zero, while the radiation stress does not have the surface roller contribution. Equations (A4)–(A6) can be solved numerically using the conjugate gradient algorithm modified from that used by *Casulli and Cheng* [1992] for Cartesian grids, given sufficient boundary conditions (wind stresses, river inflows, precipitation, and open boundary water elevation), initial conditions (water level), and other data (bathymetry and topography). In practical applications, it is possible to solve only the vertically integrated 2-D version of the CH3D model, instead of solving the complete 3-D equations. The 2-D model generally results in significant saving in computational time and comparable water level simulation in shallow coastal regions.

## A2. Boundary Conditions for the Coastal Surge Model CH3D

[71] The boundary condition at the free surface is calculated using

$$\tau_x^w = \rho_a C_d u_w W_s \quad (\text{A7})$$

$$\tau_y^w = \rho_a C_d v_w W_s \quad (\text{A8})$$

where  $u_w$  and  $v_w$  are wind speed components, and  $W_s$  is the total wind speed. The drag coefficient,  $C_d$  is calculated using the *Garratt* [1977] formulation:

$$C_d = 0.001 \times (0.75 + 0.067W_s) \quad (\text{A9})$$

When waves are present, the drag coefficient is calculated following the *Donelan et al.* [1993] formula described in equations (1) and (2).

[72] The boundary condition at the bottom is expressed in terms of bottom stress given by the quadratic law:

$$\tau_{bx} = \rho_w C_d u_b \sqrt{u_b^2 + v_b^2} \quad (\text{A10})$$

$$\tau_{by} = \rho_w C_d v_b \sqrt{u_b^2 + v_b^2} \quad (\text{A11})$$

where  $u_b$  and  $v_b$  are bottom velocities and  $C_d$  is the drag coefficient which is defined using the formulation by *Sheng* [1983]:

$$C_d = \left[ \frac{\kappa}{\ln(z_1/z_0)} \right]^2 \quad (\text{A12})$$

where  $\kappa$  is the von Karman constant. The formulation states that the coefficient is a function of the size of the bottom roughness,  $z_0$ , and the height at which  $u_b$  is measured,  $z_1$  is within the constant flux layer above the bottom. The size of

the bottom roughness can be expressed in terms of the Nikuradse equivalent sand grain size,  $k_s$ , using the relation  $z_0 = k_s/30$ .

[73] In the two-dimensional mode, the bottom boundary conditions are given using the Chezy-Manning formulation:

$$\tau_{bx} = \rho A_v \frac{\partial u_b}{\partial z} = \frac{g u_b \sqrt{u_b^2 + v_b^2}}{C_z^2} \quad (\text{A13})$$

$$\tau_{by} = \rho A_v \frac{\partial v_b}{\partial z} = \frac{g v_b \sqrt{u_b^2 + v_b^2}}{C_z^2} \quad (\text{A14})$$

where  $C_z$  is the Chezy friction coefficient defined as

$$C_z = 4.64 \frac{R^{1/6}}{n} \quad (\text{A15})$$

where  $R$  is the hydraulic radius which can be approximated by the total depth given in centimeters, and  $n$  is Manning's  $n$ .

[74] **Acknowledgments.** We appreciate the partial support of Florida Sea Grant project R/C-S47, SURA, and NOAA IOOS grant NA07NOS47302111. We thank H. Chen of NOAA for providing the WAVEWATCH-III data, H. Graber of University of Miami for providing the WINDGEN data, L. Brasseur of VIMS for providing the wave and current data at Gloucester Point, and K. Hathaway and B. Birkemeier of USACE/FRF for providing the ADCP data at Kitty Hawk. We also appreciate the comments of two anonymous reviewers.

## References

- Alymov, V. (2005), Integrated modeling of storm surges during Hurricanes Isabel, Charley, and Frances, Ph.D. dissertation, Univ. of Fla., Gainesville.
- Battjes, J. A. (1975), A note on modeling of turbulence in the surf-zone, in *Symposium on Modeling Techniques*, pp. 1050–1061, Am. Soc. of Civ. Eng., Reston, Va.
- Bijker, E. W. (1966), The increase of bed shear in a current due to wave action, in *Proceedings of the 10th International Conference on Coastal Engineering*, pp. 746–765, Am. Soc. of Civ. Eng., Reston, Va.
- Bijker, E. W. (1986), Scour around structures, in *Proceedings of the 21st International Conference on Coastal Engineering*, pp. 1754–1768, Am. Soc. of Civ. Eng., Reston, Va.
- Blumberg, A., and G. L. Mellor (1987), A description of a three-dimensional coastal ocean circulation model, in *Three-Dimensional Coastal Ocean Models, Coastal Estuarine Sci.*, vol. 4, edited by N. S. Heaps, pp. 1–16, AGU, Washington, D. C.
- Bode, L., and T. A. Hardy (1997), Progress and prospects in storm surge modeling, *J. Hydraul. Eng.*, 123, 315–331, doi:10.1061/(ASCE)0733-9429(1997)123:4(315).
- Booij, N., R. C. Ris, and L. H. Holthuijsen (1999), A third-generation wave model for coastal regions: 1. Model description and validation, *J. Geophys. Res.*, 104, 7649–7666, doi:10.1029/98JC02622.
- Casulli, V., and R. T. Cheng (1992), Semi-implicit finite difference methods for three-dimensional shallow water flow, *Int. J. Numer. Methods Fluids*, 15, 629–648, doi:10.1002/flid.1650150602.
- Casulli, V., and R. A. Walters (2000), An unstructured, three-dimensional model based on the shallow water equations, *Int. J. Numer. Methods Fluids*, 32, 331–348, doi:10.1002/(SICI)1097-0363(20000215)32:3<331::AID-FLD941>3.0.CO;2-C.
- Davis, J. R., and Y. P. Sheng (2003), Development of a parallel storm surge model, *Int. J. Numer. Methods Fluids*, 42, 549–580, doi:10.1002/flid.531.
- De Vriend, H. J., and M. J. F. Stive (1987), Quasi-3D modelling of near-shore currents, *Coastal Eng.*, 11, 565–601, doi:10.1016/0378-3839(87)90027-5.
- Donelan, M. A., F. W. Dobson, S. D. Smith, and R. J. Anderson (1993), On the dependence of sea-surface roughness on wave development, *J. Phys. Oceanogr.*, 23, 2143–2149, doi:10.1175/1520-0485(1993)023<2143:OTDOSS>2.0.CO;2.

- Flather, R. A. (1994), A storm prediction model for the northern Bay of Bengal with application to the cyclone disaster in April 1991, *J. Phys. Oceanogr.*, *24*, 172–190, doi:10.1175/1520-0485(1994)024<0172:ASSPMF>2.0.CO;2.
- Foreman, M. G. G. (1977), Manual for tidal heights analysis and prediction, *Pac. Mar. Sci. Rep.* 77-10, Inst. of Ocean Sci., Patricia Bay, Sidney, B. C.
- Garratt, J. R. (1977), Review of drag coefficients over oceans and continents, *Mon. Weather Rev.*, *105*, 915–929, doi:10.1175/1520-0493(1977)105<0915:RODCOO>2.0.CO;2.
- Graber, H. C., V. J. Cardone, R. E. Jensen, D. N. Slinn, S. C. Hagen, A. T. Cox, M. D. Powell, and C. Grassl (2006), Coastal forecasts and storm surge predictions for tropical cyclones: A timely partnership program, *Oceanography*, *19*, 130–141.
- Grant, W. D., and O. S. Madsen (1979), Combined wave and current interaction with a rough bottom, *J. Geophys. Res.*, *84*, 1797–1808, doi:10.1029/JC084iC04p01797.
- Haas, K. A., and I. A. Svendsen (2000), Three-dimensional modeling of rip current systems, *Rep. CACR-00-06*, 250 pp., Cent. for Appl. Coastal Res., Univ. of Del., Newark.
- Holland, G. (1980), An analytic model of the wind and pressure profiles in hurricanes, *Mon. Weather Rev.*, *108*, 1212–1218, doi:10.1175/1520-0493(1980)108<1212:AAMOTW>2.0.CO;2.
- Houston, S. H., W. A. Shaffer, M. D. Powell, and J. Chen (1999), Comparisons of HRD and SLOSH surface wind fields in hurricanes: Implications for storm surge modeling, *Weather Forecast.*, *14*, 671–686, doi:10.1175/1520-0434(1999)014<0671:COHASS>2.0.CO;2.
- Hubbert, G. D., and K. L. McInnes (1999), A storm surge inundation model for coastal planning and impact studies, *J. Coastal Res.*, *15*, 168–185.
- Interagency Performance Evaluation Taskforce (IPET) (2006), Performance evaluation of the New Orleans and Southeast Louisiana hurricane protection system, technical report, U.S. Army Corps of Eng., Vicksburg, Miss.
- Jelesnianski, C. P., J. Chen, and W. A. Shaffer (1992), SLOSH: Sea, Lake, and Overland Surges from Hurricane Phenomena, *NOAA Tech. Rep. NWS 48*, Natl. Weather Serv., Silver Spring, Md.
- Komen, G. J., L. Cavaleri, M. Donelan, K. Hasselmann, S. Hasselmann, and P. A. E. M. Janssen (1994), *Dynamics and Modelling of Ocean Waves*, 532 pp., Cambridge Univ. Press, New York.
- Lee, J., and Y. P. Sheng (2008), Simulation of storm surge induced by Hurricane Ivan using an unstructured grid hydrodynamic model, paper presented at the 2008 Ocean Sciences Meeting, Am. Soc. of Limnol. and Oceanogr., Orlando, Fla.
- Li, M., L. Zhong, W. C. Boicourt, S. Zhang, and D.-L. Zhang (2006), Hurricane-induced storm surges, currents and destratification in a semi-enclosed bay, *Geophys. Res. Lett.*, *33*, L02604, doi:10.1029/2005GL024992.
- Longuet-Higgins, M. S., and R. W. Stewart (1964), Radiation stresses in water waves: A physical discussion, with applications, *Deep Sea Res.*, *11*, 529–562.
- Luettich, R., J. J. Westerink, and N. W. Scheffner (1992), ADCIRC: An advanced three-dimensional circulation model for shelves coasts and estuaries, report 1: Theory and methodology of ADCIRC-2DDI and ADCIRC-3DL, *Dredging Res. Program Tech. Rep. DRP-92-6*, U.S. Army Corps of Eng., Washington, D. C.
- Mastenbroek, C., G. Burgers, and P. A. E. M. Janssen (1993), The dynamical coupling of a wave model and a storm-surge model through the atmospheric boundary-layer, *J. Phys. Oceanogr.*, *23*, 1856–1866, doi:10.1175/1520-0485(1993)023<1856:TDCOAW>2.0.CO;2.
- Mellor, G. (2003), The three-dimensional current and surface wave equation, *J. Phys. Oceanogr.*, *33*, 1978–1989, doi:10.1175/1520-0485(2003)033<1978:TTCASW>2.0.CO;2.
- Mellor, G. (2008), The depth-dependent current and wave interaction equations: A revision, *J. Phys. Oceanogr.*, *38*, 2587–2596, doi:10.1175/2008JPO3971.1.
- Morey, S. L., S. Baig, M. A. Bourassa, D. S. Dukhovskoy, and J. J. O'Brien (2006), Remote forcing contribution to storm-induced sea level rise during Hurricane Dennis, *Geophys. Res. Lett.*, *33*, L19603, doi:10.1029/2006GL027021.
- Mukai, A. Y., J. J. Westerink, and R. A. Luettich (2002), Guidelines for using the East Coast 2001 database of tidal constituents within the western North Atlantic Ocean, Gulf of Mexico and Caribbean Sea, *Coastal and Hydraul. Eng. Tech. Note IV-XX*, U.S. Army Corps of Eng., Washington, D. C.
- NOAA (2004), National Weather Service service assessment: Hurricane Isabel September 18–19, 2003, Silver Spring, Md.
- Preller, R. H., P. G. Posey, and G. M. Dawson (2005), Hurricane Isabel: A numerical model study of storm surge along the east coast of the United States, paper presented at 6th Conference on Coastal Atmospheric and Oceanic Prediction and Processes, San Diego, Calif., 9–13 Jan.
- Shen, J., H. Wang, M. Sisson, and W. Gong (2006), Storm tide simulation in the Chesapeake Bay using an unstructured grid model, *Estuarine Coastal Shelf Sci.*, *68*, 1–16, doi:10.1016/j.ecss.2005.12.018.
- Sheng, Y. P. (1983), Mathematical modeling of three-dimensional coastal currents and sediment dispersion: Model development and application, *Tech. Rep. CERC-83-2*, Aeronaut. Res. Assoc. of Princeton, Princeton, N. J.
- Sheng, Y. P. (1987), On modeling three-dimensional estuarine and marine hydrodynamics, in *Three-Dimensional Models of Marine and Estuarine Dynamics*, edited by B. M. Jamart, pp. 35–54, Elsevier, New York.
- Sheng, Y. P. (1990), Evolution of a three-dimensional curvilinear-grid hydrodynamic model for estuaries, lakes and coastal waters: CH3D, in *Estuarine and Coastal Modeling 1990*, edited by M. L. Spaulding, pp. 40–49, Am. Soc. of Civ. Eng., Reston, Va.
- Sheng, Y. P., and W. Lick (1979), The transport and resuspension of sediments in a shallow lake, *J. Geophys. Res.*, *84*, 1809–1826, doi:10.1029/JC084iC04p01809.
- Sheng, Y. P., and C. Villaret (1989), Modeling the effect of suspended sediment stratification on bottom exchange process, *J. Geophys. Res.*, *94*, 14,429–14,444, doi:10.1029/JC094iC10p14429.
- Sheng, Y. P., V. Alymov, V. Paramygin, and J. R. Davis (2006), An integrated modeling system for forecasting of storm surge and coastal inundation, in *Estuarine and Coastal Modeling IX*, edited by M. L. Spaulding, pp. 585–602, Am. Soc. of Civ. Eng., Reston, Va.
- Signell, R. P., R. C. Beardsley, H. C. Graber, and A. Capotondi (1990), Effect of wave-current interaction on steady wind-driven circulation in narrow, shallow embayments, *J. Geophys. Res.*, *95*, 9671–9678, doi:10.1029/JC095iC06p09671.
- Song, Y., and D. B. Haidvogel (1994), A semi-implicit ocean circulation model using a generalized topography-following coordinate system, *J. Comput. Phys.*, *115*, 228–244, doi:10.1006/jcph.1994.1189.
- Svendsen, I. A. (1984), Mass flux and undertow in a surf zone, *Coastal Eng.*, *8*, 347–365, doi:10.1016/0378-3839(84)90030-9.
- Svendsen, I. A. (1987), Analysis of surf zone turbulence, *J. Geophys. Res.*, *92*, 5115–5124, doi:10.1029/JC092iC05p05115.
- The Wamdi Group (1988), The WAM model—A third generation ocean wave prediction model, *J. Phys. Oceanogr.*, *18*, 1775–1810.
- Tolman, H. L. (1999), User manual and system documentation of WAVEWATCH-III version 1.18, *OMB Tech. Note 167*, Natl. Cent. for Environ. Predict., Washington, D. C.
- Valle-Levinson, A., K.-C. Wong, and K. T. Bosley (2002), Response of the lower Chesapeake Bay to forcing from Hurricane Floyd, *Cont. Shelf Res.*, *22*, 1715–1729, doi:10.1016/S0278-4343(02)00034-1.
- Zhang, M. Y., and Y. S. Li (1996), The synchronous coupling of a third-generation wave model and a two-dimensional storm surge model, *Ocean Eng.*, *23*, 533–543, doi:10.1016/0029-8018(95)00067-4.
- Zhang, Y., and Y. P. Sheng (2008), Simulation of storm surge, wave, and inundation during Hurricane Ivan using CH3D-SSMS, paper presented at the 2008 Ocean Sciences Meeting, Am. Soc. of Limnol. and Oceanogr., Orlando, Fla.

V. Alymov, V. A. Paramygin, and Y. P. Sheng, Civil and Coastal Engineering Department, University of Florida, 365 Weil Hall, P.O. Box 116580, Gainesville, FL 32611, USA. (pete@coastal.ufl.edu)